Membrane Technology and Applications, Second Edition. Richard W. Baker

ISBN: 0-470-85445-6

2 MEMBRANE TRANSPORT THEORY

Introduction

The most important property of membranes is their ability to control the rate of permeation of different species. The two models used to describe the mechanism of permeation are illustrated in Figure 2.1. One is the solution-diffusion model, in which permeants dissolve in the membrane material and then diffuse through the membrane down a concentration gradient. The permeants are separated because of the differences in the solubilities of the materials in the membrane and the differences in the rates at which the materials diffuse through the membrane. The other model is the pore-flow model, in which permeants are transported by pressure-driven convective flow through tiny pores. Separation occurs because one of the permeants is excluded (filtered) from some of the pores in the membrane through which other permeants move. Both models were proposed in the nineteenth century, but the pore-flow model, because it was closer to normal physical experience, was more popular until the mid-1940s. However, during the 1940s, the solution-diffusion model was used to explain transport of gases through polymeric films. This use of the solution-diffusion model was relatively uncontroversial, but the transport mechanism in reverse osmosis membranes was a hotly debated issue in the 1960s and early 1970s [1–6]. By 1980, however, the proponents of solution-diffusion had carried the day; currently only a few die-hard pore-flow modelers use this approach to rationalize reverse osmosis.

Diffusion, the basis of the solution-diffusion model, is the process by which matter is transported from one part of a system to another by a concentration gradient. The individual molecules in the membrane medium are in constant random molecular motion, but in an isotropic medium, individual molecules have no preferred direction of motion. Although the average displacement of an individual molecule from its starting point can be calculated, after a period of time nothing can be said about the direction in which any individual molecule will move. However, if a concentration gradient of permeate molecules is formed in the medium, simple statistics show that a net transport of matter will occur

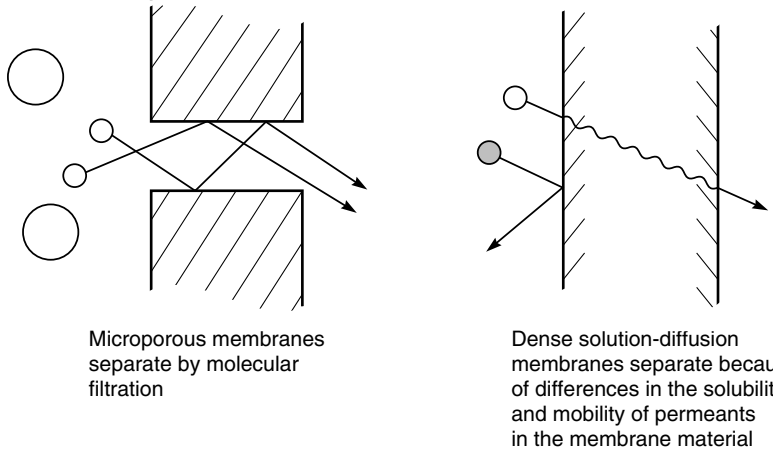

Figure 2.1 Molecular transport through membranes can be described by a flow through permanent pores or by the solution-diffusion mechanism

from the high concentration to the low concentration region. For example, when two adjacent volume elements with slightly different permeant concentrations are separated by an interface, then simply because of the difference in the number of molecules in each volume element, more molecules will move from the concentrated side to the less concentrated side of the interface than will move in the other direction. This concept was first recognized by Fick theoretically and experimentally in 1855 [7]. Fick formulated his results as the equation now called Fick's law of diffusion, which states

$$J_i = -D_i \frac{\mathrm{d}c_i}{\mathrm{d}x} \tag{2.1}$$

where J_i is the rate of transfer of component i or flux (g/cm^2 · s) and $\mathrm{d}c_i/\mathrm{d}x$ *is* the concentration gradient of component i. The term D_i is called the diffusion coefficient (cm^2/s) and is a measure of the mobility of the individual molecules. The minus sign shows that the direction of diffusion is down the concentration gradient. Diffusion is an inherently slow process. In practical diffusion-controlled separation processes, useful fluxes across the membrane are achieved by making the membranes very thin and creating large concentration gradients in the membrane.

Pressure-driven convective flow, the basis of the pore flow model, is most commonly used to describe flow in a capillary or porous medium. The basic equation covering this type of transport is Darcy's law, which can be written as

$$J_i = K' c_i \frac{\mathrm{d}p}{\mathrm{d}x} \tag{2.2}$$

where dp/dx is the pressure gradient existing in the porous medium, c_i is the concentration of component i in the medium and K' is a coefficient reflecting the nature of the medium. In general, convective-pressure-driven membrane fluxes are high compared with those obtained by simple diffusion.

The difference between the solution-diffusion and pore-flow mechanisms lies in the relative size and permanence of the pores. For membranes in which transport is best described by the solution-diffusion model and Fick's law, the free-volume elements (pores) in the membrane are tiny spaces between polymer chains caused by thermal motion of the polymer molecules. These volume elements appear and disappear on about the same timescale as the motions of the permeants traversing the membrane. On the other hand, for a membrane in which transport is best described by a pore-flow model and Darcy's law, the free-volume elements (pores) are relatively large and fixed, do not fluctuate in position or volume on the timescale of permeant motion, and are connected to one another. The larger the individual free volume elements (pores), the more likely they are to be present long enough to produce pore-flow characteristics in the membrane. As a rough rule of thumb, the transition between transient (solution-diffusion) and permanent (pore-flow) pores is in the range 5–10 Å diameter.

The average pore diameter in a membrane is difficult to measure directly and must often be inferred from the size of the molecules that permeate the membrane or by some other indirect technique. With this caveat in mind membranes can be organized into the three general groups shown in Figure 2.2:

- Ultrafiltration, microfiltration and microporous Knudsen-flow gas separation membranes are all clearly microporous, and transport occurs by pore flow.
- Reverse osmosis, pervaporation and polymeric gas separation membranes have a dense polymer layer with no visible pores, in which the separation occurs. These membranes show different transport rates for molecules as small as 2–5 Å in diameter. The fluxes of permeants through these membranes are also much lower than through the microporous membranes. Transport is best described by the solution-diffusion model. The spaces between the polymer chains in these membranes are less than 5 Å in diameter and so are within the normal range of thermal motion of the polymer chains that make up the membrane matrix. Molecules permeate the membrane through free volume elements between the polymer chains that are transient on the timescale of the diffusion processes occurring.
- Membranes in the third group contain pores with diameters between 5 Å and 10 Å and are intermediate between truly microporous and truly solution-diffusion membranes. For example, nanofiltration membranes are intermediate between ultrafiltration membranes and reverse osmosis membranes. These membranes have high rejections for the di- and trisaccharides sucrose and raffinose with molecular diameters of 10–13 Å, but freely pass the monosaccharide fructose with a molecular diameter of about 5–6 Å.

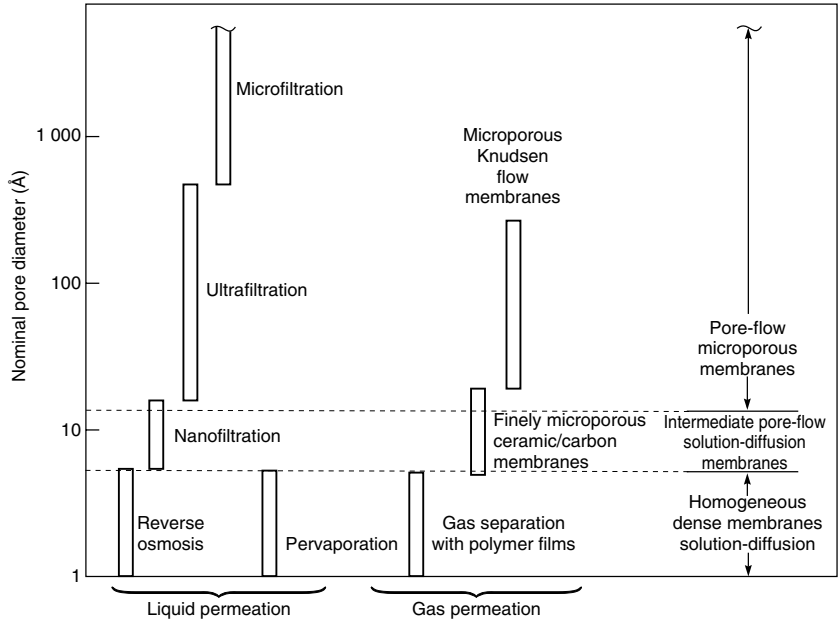

Figure 2.2 Schematic representation of the nominal pore size and best theoretical model for the principal membrane separation processes

In this chapter, permeation through dense nonporous membranes is covered first; this includes permeation in reverse osmosis, pervaporation, and gas separation membranes. Transport occurs by molecular diffusion and is described by the solution-diffusion model. The predictions of this model are in good agreement with experimental data, and a number of simple equations that usefully rationalize the properties of these membranes result. In the second part of the chapter, transport in microporous ultrafiltration and microfiltration membranes is covered more briefly. Transport through these membranes occurs by convective flow with some form of sieving mechanism producing the separation. However, the ability of theory to rationalize transport in these membranes is poor. A number of factors concurrently affect permeation, so a simple quantitative description of the process is not possible. Finally, a brief discussion of membranes that fall into the 'intermediate' category is given.

Solution-diffusion Model

Molecular Dynamics Simulations

The solution-diffusion model applies to reverse osmosis, pervaporation and gas permeation in polymer films. At first glance these processes appear to be very

different. Reverse osmosis uses a large pressure difference across the membrane to separate water from salt solutions. In pervaporation, the pressure difference across the membrane is small, and the process is driven by the vapor pressure difference between the feed liquid and the low partial pressure of the permeate vapor. Gas permeation involves transport of gases down a pressure or concentration gradient. However, all three processes involve diffusion of molecules in a dense polymer. The pressure, temperature, and composition of the fluids on either side of the membrane determine the concentration of the diffusing species at the membrane surface in equilibrium with the fluid. Once dissolved in the membrane, individual permeating molecules move by the same random process of molecular diffusion no matter whether the membrane is being used in reverse osmosis, pervaporation, or gas permeation. Often, similar membranes are used in very different processes. For example, cellulose acetate membranes were developed for desalination of water by reverse osmosis, but essentially identical membranes have been used in pervaporation to dehydrate alcohol and are widely used in gas permeation to separate carbon dioxide from natural gas. Similarly, silicone rubber membranes are too hydrophobic to be useful in reverse osmosis but are used to separate volatile organics from water by pervaporation and organic vapors from air in gas permeation.

The advent of powerful computers has allowed the statistical fluctuations in the volumes between polymer chains due to thermal motion to be calculated. Figure 2.3 shows the results of a computer molecular dynamics simulation calculation for a small-volume element of a polymer. The change in position of individual polymer molecules in a small-volume element can be calculated at short enough time intervals to represent the normal thermal motion occurring in a polymeric matrix. If a penetrant molecule is placed in one of the small-free-volume microcavities between polymer chains, its motion can also be calculated. The simulated motion of a carbon dioxide molecule in a 6FDA-4PDA polyimide matrix is shown in Figure 2.3 [8]. During the first 100 ps of the simulation, the carbon dioxide molecule bounces around in the cavity where it has been placed, never moving more than about 5 Å, the diameter of the microcavity. After 100 ps, however, a chance thermal motion moves a segment of the polymer chains sufficiently for the carbon dioxide molecule to jump approximately 10 Å to an adjacent cavity where it remains until another movement of the polymer chains allows it to jump to another cavity. By repeating these calculations many times and averaging the distance moved by the gas molecule, its diffusion coefficient can be calculated.

An alternative method of representing the movement of an individual molecule by computational techniques is shown in Figure 2.4 [9]. This figure shows the movement of three different permeate molecules over a period of 200 ps in a silicone rubber polymer matrix. The smaller helium molecule moves more frequently and makes larger jumps than the larger methane molecule. Helium, with a molecular diameter of 2.55 Å, has many more opportunities to move from one

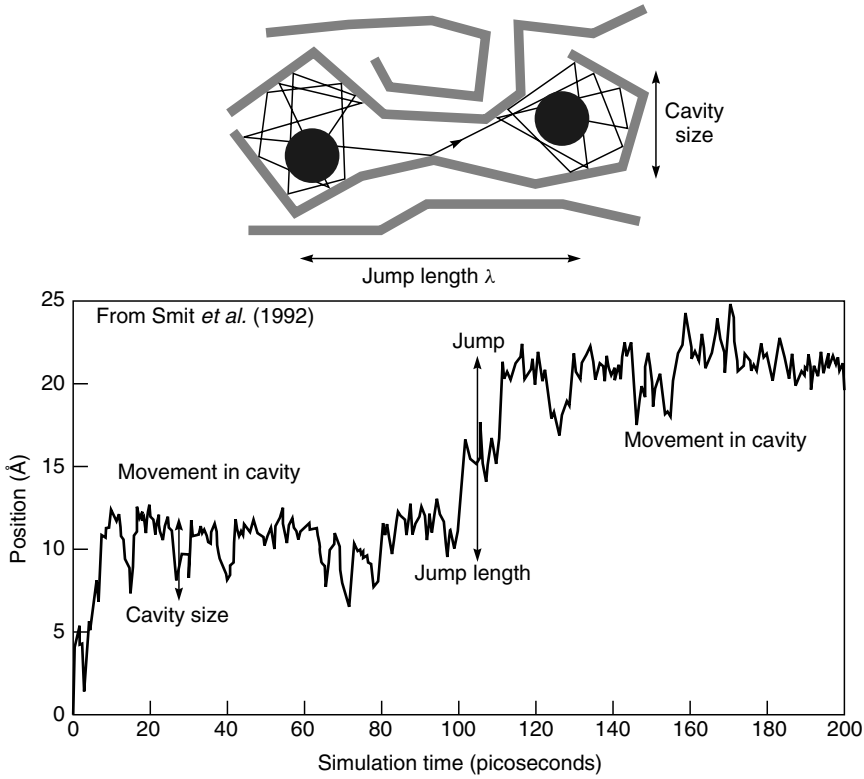

Figure 2.3 Motion of a carbon dioxide molecule in a 6FDA-4PDA polymer matrix [8]. Reprinted from *J. Membr. Sci.* **73**, E. Smit, M.H.V. Mulder, C.A. Smolders, H. Karrenbeld, J. van Eerden and D. Feil, Modeling of the Diffusion of Carbon Dioxide in Polyimide Matrices by Computer Simulation, p. 247, Copyright 1992, with permission from Elsevier

position to another than methane, with a molecular diameter of 3.76 Å. Oxygen, with a molecular diameter of 3.47 Å, has intermediate mobility. The effect of polymer structure on diffusion can be seen by comparing the distance moved by the gas molecules in the same 200-ps period in Figures 2.3 and 2.4. Figure 2.3 simulates diffusion in a glassy rigid-backbone polyimide. In 200 ps, the permeate molecule has made only one large jump. Figure 2.4 simulates diffusion in silicone rubber, a material with a very flexible polymer backbone. In 200 ps, all the permeants in silicone rubber have made a number of large jumps from one microcavity to another.

Molecular dynamics simulations also allow the transition from the solution-diffusion to the pore-flow transport mechanism to be seen. As the microcavities become larger, the transport mechanism changes from the diffusion process

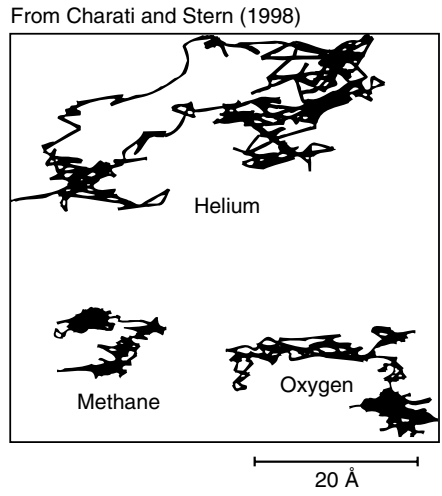

Figure 2.4 Simulated trajectories of helium, oxygen and methane molecules during a 200-ps time period in a poly(dimethylsiloxane) matrix [9]. Reprinted with permission from S.G. Charati and S.A. Stern, Diffusion of Gases in Silicone Polymers: Molecular Dynamic Simulations, *Macromolecules* **31**, 5529. Copyright 1998, American Chemical Society

simulated in Figures 2.3 and 2.4 to a pore-flow mechanism. Permanent pores form when the microcavities are larger than about 10 Å in diameter.

However, molecular dynamics calculations are at an early stage of development. Current estimates of diffusion coefficients from these simulations are generally far from matching the experimental values, and enormous computing power and a better understanding of the interactions between the molecules of polymer chains will be required to produce accurate predictions. Nonetheless, the technique demonstrates the qualitative basis of the solution-diffusion model in a very graphic way. Currently, the best quantitative description of permeation uses phenomenological equations, particularly Fick's law. This description is given in the section that follows, which outlines the mathematical basis of the solution-diffusion model. Much of this section is adapted from a 1995 *Journal of Membrane Science* article written with my colleague, Hans Wijmans [10].

Concentration and Pressure Gradients in Membranes

The starting point for the mathematical description of diffusion in membranes is the proposition, solidly based in thermodynamics, that the driving forces of pressure, temperature, concentration, and electrical potential are interrelated and that the overall driving force producing movement of a permeant is the gradient in its chemical potential. Thus, the flux, J_i(g/cm$^2 \cdot$ s), of a component, i, is

described by the simple equation

$$J_i = -L_i \frac{\mathrm{d}\mu_i}{\mathrm{d}x} \tag{2.3}$$

where $\mathrm{d}\mu_i/\mathrm{d}x$ is the chemical potential gradient of component i and L_i is a coefficient of proportionality (not necessarily constant) linking this chemical potential driving force to flux. Driving forces, such as gradients in concentration, pressure, temperature, and electrical potential can be expressed as chemical potential gradients, and their effect on flux expressed by this equation. This approach is extremely useful, because many processes involve more than one driving force, for example, both pressure and concentration in reverse osmosis. Restricting the approach to driving forces generated by concentration and pressure gradients, the chemical potential is written as

$$\mathrm{d}\mu_i = RT\,\mathrm{d}\ln(\gamma_i n_i) + \upsilon_i \mathrm{d}p \tag{2.4}$$

where n_i is the mole fraction (mol/mol) of component i, γ_i is the activity coefficient (mol/mol) linking mole fraction with activity, p is the pressure, and υ_i is the molar volume of component i.

In incompressible phases, such as a liquid or a solid membrane, volume does not change with pressure. In this case, integrating Equation (2.4) with respect to concentration and pressure gives

$$\mu_i = \mu_i^o + RT\ln(\gamma_i n_i) + \upsilon_i(p - p_i^o) \tag{2.5}$$

where μ_i^o is the chemical potential of pure i at a reference pressure, p_i^o.

In compressible gases, the molar volume changes with pressure. Using the ideal gas laws in integrating Equation (2.4) gives

$$\mu_i = \mu_i^o + RT\ln(\gamma_i n_i) + RT\ln\frac{p}{p_i^o} \tag{2.6}$$

To ensure that the reference chemical potential μ_i^o is identical in Equations (2.5) and (2.6), the reference pressure p_i^o is defined as the saturation vapor pressure of i, $p_{i_{\mathrm{sat}}}$. Equations (2.5) and (2.6) can then be rewritten as

$$\mu_i = \mu_i^o + RT\ln(\gamma_i n_i) + \upsilon_i(p - p_{i_{\mathrm{sat}}}) \tag{2.7}$$

for incompressible liquids and the membrane phase, and as

$$\mu_i = \mu_i^o + RT\ln(\gamma_i n_i) + RT\ln\frac{p}{p_{i_{\mathrm{sat}}}} \tag{2.8}$$

for compressible gases.

Several assumptions must be made to define any permeation model. Usually, the first assumption governing transport through membranes is that the fluids on

either side of the membrane are in equilibrium with the membrane material at the interface. This assumption means that the gradient in chemical potential from one side of the membrane to the other is continuous. Implicit in this assumption is that the rates of absorption and desorption at the membrane interface are much higher than the rate of diffusion through the membrane. This appears to be the case in almost all membrane processes, but may fail in transport processes involving chemical reactions, such as facilitated transport, or in diffusion of gases through metals, where interfacial absorption can be slow.

The second assumption concerns the pressure and concentration gradients in the membrane. The solution-diffusion model assumes that when pressure is applied across a dense membrane, the pressure throughout the membrane is constant at the highest value. This assumes, in effect, that solution-diffusion membranes transmit pressure in the same way as liquids. Consequently, the solution-diffusion model assumes that the pressure within a membrane is uniform and that the chemical potential gradient across the membrane is expressed only as a concentration gradient [5,10]. The consequences of these two assumptions are illustrated in Figure 2.5, which shows pressure-driven permeation of a one-component solution through a membrane by the solution-diffusion mechanism.

In the solution-diffusion model, the pressure within the membrane is constant at the high-pressure value (p_o), and the gradient in chemical potential across the membrane is expressed as a smooth gradient in solvent activity ($\gamma_i n_i$). The flow that occurs down this gradient is expressed by Equation (2.3), but because no pressure gradient exists within the membrane, Equation (2.3) can be rewritten by combining Equations (2.3) and (2.4). Assuming γ_i is constant, this gives

$$J_i = -\frac{RTL_i}{n_i} \cdot \frac{\mathrm{d}n_i}{\mathrm{d}x} \tag{2.9}$$

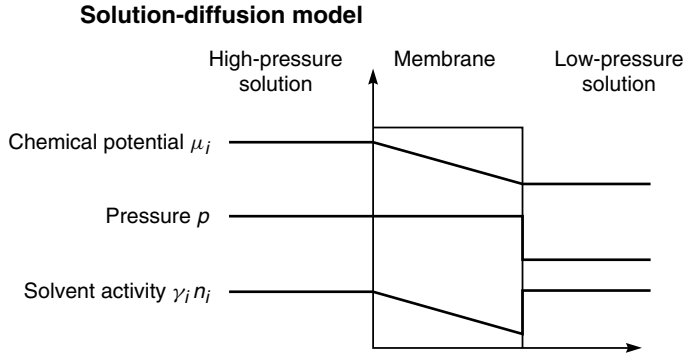

Figure 2.5 Pressure driven permeation of a one-component solution through a membrane according to the solution-diffusion transport model

In Equation (2.9), the gradient of component i across the membrane is expressed as a gradient in mole fraction of component i. Using the more practical term concentration c_i (g/cm^3) defined as

$$c_i = m_i \rho n_i \tag{2.10}$$

where m_i is the molecular weight of i (g/mol) and ρ is the molar density (mol/cm^3), Equation (2.9) can be written as

$$J_i = -\frac{RTL_i}{c_i} \cdot \frac{\mathrm{d}c_i}{\mathrm{d}x} \tag{2.11}$$

Equation (2.11) has the same form as Fick's law in which the term RTL_i/c_i can be replaced by the diffusion coefficient D_i. Thus,

$$J_i = -D_i \frac{\mathrm{d}c_i}{\mathrm{d}x} \tag{2.12}$$

Integrating over the thickness of the membrane then gives[1]

$$J_i = \frac{D_i(c_{i_{o(m)}} - c_{i_{\ell(m)}})}{\ell} \tag{2.13}$$

By using osmosis as an example, concentration and pressure gradients according to the solution-diffusion model can be discussed in a somewhat more complex situation. The activity, pressure, and chemical potential gradients within this type of membrane are illustrated in Figure 2.6.

Figure 2.6(a) shows a semipermeable membrane separating a salt solution from the pure solvent. The pressure is the same on both sides of the membrane. For simplicity, the gradient of salt (component j) is not shown in this figure, but the membrane is assumed to be very selective, so the concentration of salt within the membrane is small. The difference in concentration across the membrane results in a continuous, smooth gradient in the chemical potential of the water (component i) across the membrane, from μ_{i_ℓ} on the water side to μ_{i_o} on the salt side. The pressure within and across the membrane is constant (that is, $p_o = p_m = p_\ell$) and the solvent activity gradient ($\gamma_{i_{(m)}} n_{i_{(m)}}$) falls continuously from the pure water (solvent) side to the saline (solution) side of the membrane. Consequently, water passes across the membrane from right to left.

Figure 2.6(b) shows the situation at the point of osmotic equilibrium, when sufficient pressure has been applied to the saline side of the membrane to bring the flow across the membrane to zero. As shown in Figure 2.6(b), the pressure

[1]In the equations that follow, the terms i and j represent components of a solution, and the terms o and ℓ represent the positions of the feed and permeate interfaces, respectively, of the membrane. Thus the term c_{i_o} represents the concentration of component i in the fluid (gas or liquid) in contact with the membrane at the feed interface. The subscript m is used to represent the membrane phase. Thus, $c_{i_{o(m)}}$ is the concentration of component i in the membrane at the feed interface (point o).

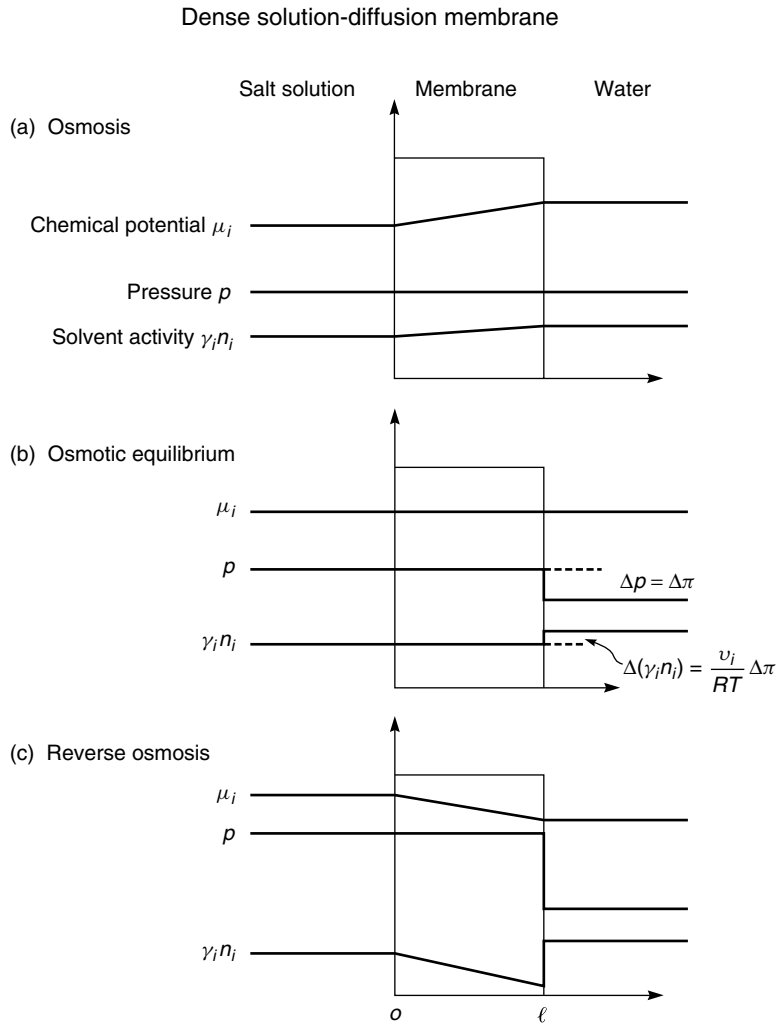

Figure 2.6 Chemical potential, pressure, and solvent activity profiles through an osmotic membrane following the solution-diffusion model. The pressure in the membrane is uniform and equal to the high-pressure value, so the chemical potential gradient within the membrane is expressed as a concentration gradient

within the membrane is assumed to be constant at the high-pressure value (p_o). There is a discontinuity in pressure at the permeate side of the membrane, where the pressure falls abruptly from p_o to p_ℓ, the pressure on the solvent side of the membrane. This pressure difference ($p_o - p_\ell$) can be expressed in terms of the chemical potential difference between the feed and permeate solutions.

The membrane in contact with the permeate-side solution is in equilibrium with this solution. Thus, Equation (2.7) can be used to link the two phases in terms of their chemical potentials, that is

$$\mu_{i_{\ell(m)}} = \mu_{i_\ell} \tag{2.14}$$

and so

$$RT \ln(\gamma_{i_{\ell(m)}} n_{i_{\ell(m)}}) + \upsilon_i p_o = RT \ln(\gamma_{i_\ell} n_{i_\ell}) + \upsilon_i p_\ell \tag{2.15}$$

On rearranging, this gives

$$RT \ln(\gamma_{i_{\ell(m)}} n_{i_{\ell(m)}}) - RT \ln(\gamma_{i_\ell} n_{i_\ell}) = -\upsilon_i (p_o - p_\ell) \tag{2.16}$$

At osmotic equilibrium $\Delta(\gamma_i n_i)$ can also be defined by

$$\Delta(\gamma_i n_i) = \gamma_{i_\ell} n_{i_\ell} - \gamma_{i_{\ell(m)}} n_{i_{\ell(m)}} \tag{2.17}$$

and, since $\gamma_{i_\ell} n_{i_\ell} \approx 1$, it follows, on substituting Equation (2.17) into (2.16), that

$$RT \ln[1 - \Delta(\gamma_i n_i)] = -\upsilon_i (p_o - p_\ell) \tag{2.18}$$

Since $\Delta(\gamma_i n_i)$ is small, $\ln[1 - \Delta(\gamma_i n_i)] \approx \Delta(\gamma_i n_i)$, and Equation (2.18) reduces to

$$\Delta(\gamma_i n_i) = \frac{-\upsilon_i (p_o - p_\ell)}{RT} = \frac{-\upsilon_i \Delta\pi}{RT} \tag{2.19}$$

Thus, the pressure difference, $(p_o - p_\ell) = \Delta\pi$, across the membrane balances the solvent activity difference $\Delta(\gamma_i n_i)$ across the membrane, and the flow is zero.

If a pressure higher than the osmotic pressure is applied to the feed side of the membrane, as shown in Figure 2.6(c), then the solvent activity difference across the membrane increases further, resulting in a flow from left to right. This is the process of reverse osmosis.

The important conclusion illustrated by Figures 2.5 and 2.6 is that, although the fluids on either side of a membrane may be at different pressures and concentrations, within a perfect solution-diffusion membrane, there is no pressure gradient—only a concentration gradient. Flow through this type of membrane is expressed by Fick's law, Equation (2.13).

Application of the Solution-diffusion Model to Specific Processes

In this section the solution-diffusion model is used to describe transport in dialysis, reverse osmosis, gas permeation and pervaporation membranes. The resulting equations, linking the driving forces of pressure and concentration with flow, are then shown to be consistent with experimental observations.

The general approach is to use the first assumption of the solution-diffusion model, namely, that the chemical potential of the feed and permeate fluids are

in equilibrium with the adjacent membrane surfaces. From this assumption, the chemical potential in the fluid and membrane phases can be equated using the appropriate expressions for chemical potential given in Equations (2.7) and (2.8). By rearranging these equations, the concentrations of the different species in the membrane at the fluids interface ($c_{i_{o(m)}}$ and $c_{i_{\ell(m)}}$) can be obtained in terms of the pressure and composition of the feed and permeate fluids. These values for $c_{i_{o(m)}}$ and $c_{i_{\ell(m)}}$ can then be substituted into the Fick's law expression, Equation (2.13), to give the transport equation for the particular process.

Dialysis

Dialysis is the simplest application of the solution-diffusion model because only concentration gradients are involved. In dialysis, a membrane separates two solutions of different compositions. The concentration gradient across the membrane causes a flow of solute and solvent from one side of the membrane to the other.

Following the general procedure described above, equating the chemical potentials in the solution and membrane phase at the feed-side interface of the membrane gives

$$\mu_{i_o} = \mu_{i_{o(m)}} \tag{2.20}$$

Substituting the expression for the chemical potential of incompressible fluids from Equation (2.7) gives

$$\mu_i^o + RT \ln(\gamma_{i_o}^{\mathrm{L}} n_{i_o}) + \upsilon_i (p_o - p_{i_{\mathrm{sat}}}) = \mu_i^o + RT \ln(\gamma_{i_{o(m)}} n_{i_{o(m)}}) + \upsilon_{i_{o(m)}} (p_o - p_{i_{\mathrm{sat}}}) \tag{2.21}$$

which leads to[2]

$$\ln(\gamma_{i_o}^{\mathrm{L}} n_{i_o}) = \ln(\gamma_{i_{o(m)}} n_{i_{o(m)}}) \tag{2.22}$$

and thus

$$n_{i_{o(m)}} = \frac{\gamma_{i_o}^{\mathrm{L}}}{\gamma_{i_{o(m)}}} \cdot n_{i_o} \tag{2.23}$$

or from Equation (2.10)

$$c_{i_{o(m)}} = \frac{\gamma_{i_o} \rho_m}{\gamma_{i_{o(m)}} \rho_o} \cdot c_{i_o} \tag{2.24}$$

Hence, defining a sorption coefficient K_i^{L} as

$$K_i^{\mathrm{L}} = \frac{\gamma_{i_o} \rho_m}{\gamma_{i_{o(m)}} \rho_o} \tag{2.25}$$

Equation (2.24) becomes

$$c_{i_{o(m)}} = K_i^{\mathrm{L}} \cdot c_{i_o} \tag{2.26}$$

[2]The superscripts G and L are used here and later to distinguish between gas phase and liquid phase activity coefficients, sorption coefficients and permeability coefficients.

From Theeuwes *et al.* (1978)

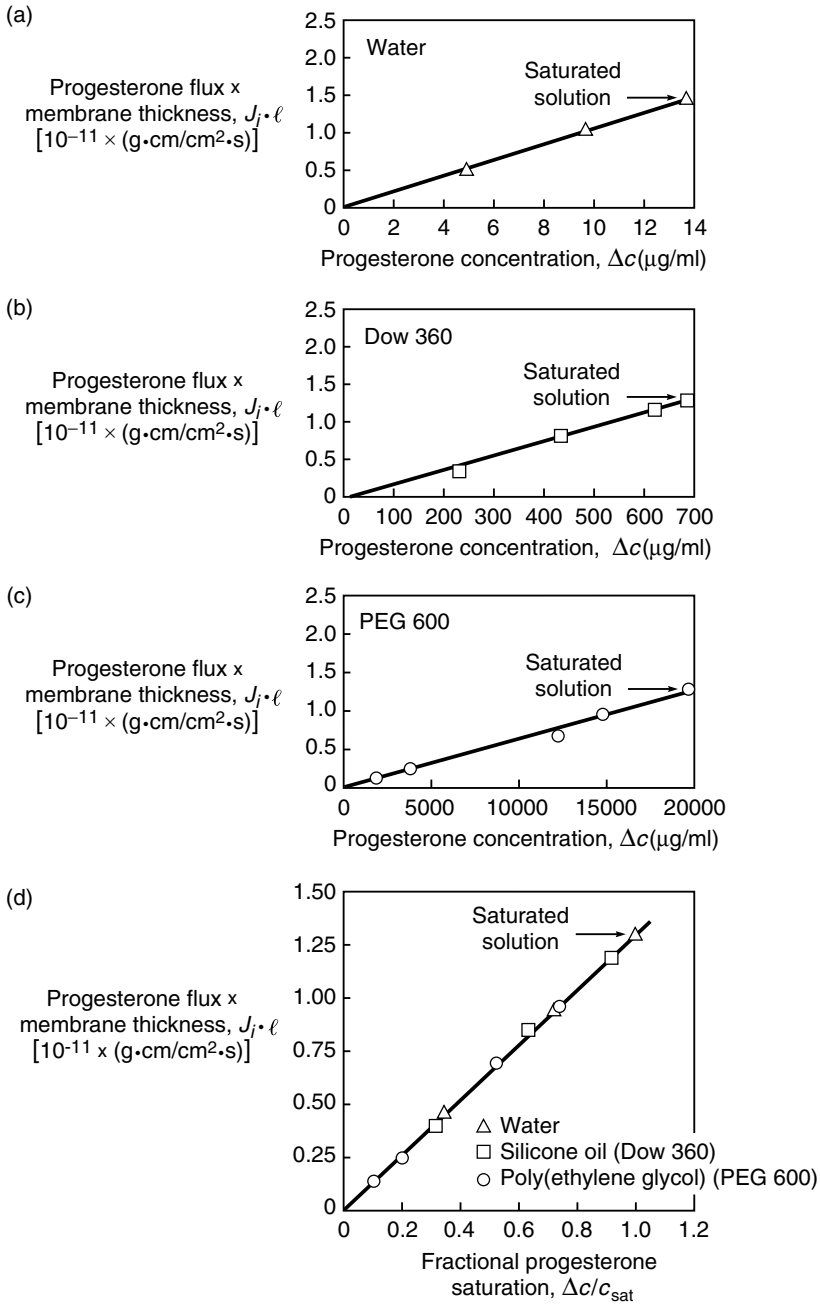

On the permeate side of the membrane, the same procedure can be followed, leading to an equivalent expression

$$c_{i_{\ell(m)}} = K_i^{\mathrm{L}} \cdot c_{i_\ell} \tag{2.27}$$

The concentrations of permeant within the membrane phase at the two interfaces can then be substituted from Equations (2.26) and (2.27) into the Fick's law expression, Equation (2.13), to give the familiar expression describing permeation through dialysis membranes:

$$J_i = \frac{D_i K_i^{\mathrm{L}}}{\ell}(c_{i_o} - c_{i_\ell}) = \frac{P_i^{\mathrm{L}}}{\ell}(c_{i_o} - c_{i_\ell}) \tag{2.28}$$

The product $D_i K_i^{\mathrm{L}}$ is normally referred to as the permeability coefficient, P_i^{L}. For many systems, D_i, K_i^{L}, and thus P_i^{L} are concentration dependent. Thus, Equation (2.28) implies the use of values for D_i, K_i^{L}, and P_i^{L} that are averaged over the membrane thickness.

The permeability coefficient P_i^{L} is often treated as a pure materials constant, depending only on the permeant and the membrane material, but in fact the nature of the solvent used in the liquid phase is also important. From Equations (2.28) and (2.25), P_i^{L} can be written as

$$P_i^{\mathrm{L}} = D_i \cdot \gamma_i^{\mathrm{L}} / \gamma_{i(m)} \cdot \frac{\rho_m}{\rho_o} \tag{2.29}$$

The presence of the term γ_i^{L} makes the permeability coefficient a function of the solvent used as the liquid phase. Some experimental data illustrating this effect are shown in Figure 2.7 [11], which is a plot of the product of the progesterone flux and the membrane thickness, $J_i \ell$ against the concentration difference across the membrane, $(c_{i_o} - c_{i_\ell})$. From Equation (2.28), the slope of this line is the permeability, P_i^L. Three sets of dialysis permeation experiments are reported, in which the solvent used to dissolve the progesterone is water, silicone oil and poly(ethylene glycol) MW 600 (PEG 600), respectively. The permeability calculated from these plots varies from 9.5×10^{-7} cm^2/s for water to 6.5×10^{-10} cm^2/s for PEG 600. This difference reflects the activity term γ_i^{L} in Equation (2.28). However, when the driving force across the membrane is

Figure 2.7 Permeation of progesterone through polyethylene vinyl acetate films. The thickness-normalized progesterone flux $(J_i \cdot \ell)$ is plotted against the progesterone concentration across the membrane, Δc [11]. The solvents for the progesterone are (a) water, (b) silicone oil and (c) poly(ethylene glycol) (PEG 600). Because of the different solubilities of progesterone in these solvents, the permeabilities calculated from these data through Equation (2.28) vary 1000-fold. All the data can be rationalized onto a single curve by plotting the thickness-normalized flux against fractional progesterone saturation as described in the text and shown in (d). The slope of this line, $P_i^{\mathrm{L}} c_{\mathrm{sat}}$ or $D_i m_i \rho_m / \gamma_{i_{(m)}}$ is a materials property dependent only on the membrane material and the permeant and independent of the solvent

represented not as a difference in concentration but as a difference in fractional saturation between the feed and permeate solution, all the data fall on a single line as shown in Figure 2.7(d). The slope of this line is the term $P_i^{\mathrm{L}} c_{\mathrm{sat}}$. This result is also in agreement with Equation (2.29), which when combined with the approximation that, for dilute solutions, the activity of component i can be written as

$$\gamma_i^{\mathrm{L}} = \frac{1}{n_{i_{\mathrm{sat}}}} = \frac{m_i \rho_o}{c_{i_{\mathrm{sat}}}} \tag{2.30}$$

yields

$$P_i^{\mathrm{L}} c_{i_{\mathrm{sat}}} = \frac{D_i m_i \rho_m}{\gamma_{i_{(m)}}} \tag{2.31}$$

The terms $D_i m_i \rho_m / \gamma_{i_{(m)}}$ and, therefore, $P_i^{\mathrm{L}} c_{\mathrm{sat}}$ are determined solely by the permeant and the membrane material and are thus independent of the liquid phase surrounding the membrane.

Reverse Osmosis

Reverse osmosis and normal osmosis (dialysis) are directly related processes. In simple terms, if a selective membrane (i.e., a membrane freely permeable to water, but much less permeable to salt) separates a salt solution from pure water, water will pass through the membrane from the pure water side of the membrane into the side less concentrated in water (salt side) as shown in Figure 2.8. This process is called normal osmosis. If a hydrostatic pressure is applied to the salt side of the membrane, the flow of water can be retarded and, when the applied pressure is sufficient, the flow ceases. The hydrostatic pressure required to stop

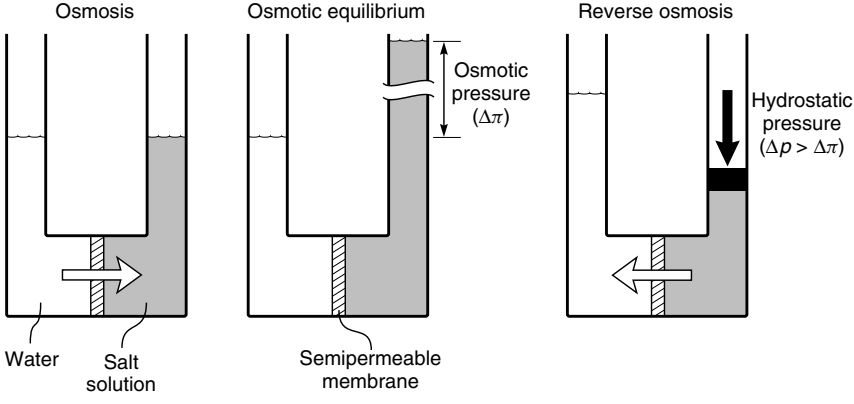

Figure 2.8 A schematic illustration of the relationship between osmosis (dialysis), osmotic equilibrium and reverse osmosis

the water flow is called the osmotic pressure ($\Delta\pi$). If pressures greater than the osmotic pressure are applied to the salt side of the membrane, then the flow of water is reversed, and water begins to flow from the salt solution to the pure water side of the membrane. This process is called reverse osmosis, which is an important method of producing pure water from salt solutions.

Reverse osmosis usually involves two components, water (i) and salt (j). Following the general procedure, the chemical potentials at both sides of the membrane are first equated. At the feed interface, the pressure in the feed solution and within the membrane are identical (as shown in Figure 2.6c). Equating the chemical potentials at this interface gives the same expression as in dialysis [cf. Equation (2.26)]

$$c_{i_{o(m)}} = K_i^{\mathrm{L}} \cdot c_{i_o} \tag{2.32}$$

A pressure difference exists at the permeate interface (as shown in Figure 2.6c) from p_o within the membrane to p_ℓ in the permeate solution. Equating the chemical potentials across this interface gives

$$\mu_{i_\ell} = \mu_{i_{\ell(m)}} \tag{2.33}$$

Substituting the appropriate expression for the chemical potential of an incompressible fluid to the liquid and membrane phases [Equation (2.7)] yields

$$\mu_i^o + RT \ln(\gamma_{i_\ell}^{\mathrm{L}} n_{i_\ell}) + \upsilon_i(p_\ell - p_{i_{\mathrm{sat}}}) = \mu_i^o + RT \ln(\gamma_{i_{\ell(m)}} n_{i_{\ell(m)}}) + \upsilon_i(p_o - p_{i_{\mathrm{sat}}}) \tag{2.34}$$

which leads to

$$\ln(\gamma_{i_\ell}^{\mathrm{L}} n_{i_\ell}) = \ln(\gamma_{i_{\ell(m)}}^{\mathrm{L}} n_{i_{\ell(m)}}) + \frac{\upsilon_i(p_o - p_\ell)}{RT} \tag{2.35}$$

Rearranging and substituting for the sorption coefficient, K_i^{L} [Equations (2.10) and (2.25)], gives the expression

$$c_{i_{\ell(m)}} = K_i^{\mathrm{L}} \cdot c_{i_\ell} \cdot \exp\left[\frac{-\upsilon_i(p_o - p_\ell)}{RT}\right] \tag{2.36}$$

The expressions for the concentrations within the membrane at the interface in Equations (2.32) and (2.36) can now be substituted into the Fick's law expression, Equation (2.13), to yield

$$J_i = \frac{D_i K_i^{\mathrm{L}}}{\ell}\left\{c_{i_o} - c_{i_\ell} \exp\left[\frac{-\upsilon_i(p_o - p_\ell)}{RT}\right]\right\} \tag{2.37}$$

Equation (2.37) and the equivalent expression for component j give the water flux and the salt flux across the reverse osmosis membrane in terms of the pressure and concentration difference across the membrane. There is an analytical expression for Equation (2.37) for a two-component feed mixture that allows the performance of the membrane to be calculated for known permeabilities, $D_i K_i^{\mathrm{L}}/\ell$ and $D_j K_j^{\mathrm{L}}/\ell$, and feed concentrations, c_{i_o} and c_{j_o}. However, more commonly

Equation (2.37) is simplified by assuming that the membrane selectivity is high, that is, $D_i K_i^{\mathrm{L}}/\ell \gg D_j K_j^{\mathrm{L}}/\ell$. This is a good assumption for most of the reverse osmosis membranes used to separate salts from water. Consider the water flux first. At the point at which the applied hydrostatic pressure balances the water activity gradient, that is, the point of osmotic equilibrium in Figure 2.6(b), the flux of water across the membrane is zero. Equation (2.37) becomes

$$J_i = 0 = \frac{D_i K_i^{\mathrm{L}}}{\ell}\left\{c_{i_o} - c_{i_\ell}\exp\left[\frac{-\upsilon_i(\Delta\pi)}{RT}\right]\right\} \tag{2.38}$$

and, on rearranging

$$c_{i_\ell} = c_{i_o}\exp\left[\frac{\upsilon_i(\Delta\pi)}{RT}\right] \tag{2.39}$$

At hydrostatic pressures higher than $\Delta\pi$, Equations (2.37) and (2.39) can be combined to yield

$$J_i = \frac{D_i K_i^{\mathrm{L}} c_{i_o}}{\ell}\left(1 - \exp\left\{\frac{-\upsilon_i[(p_o - p_\ell) - \Delta\pi]}{RT}\right\}\right) \tag{2.40}$$

or

$$J_i = \frac{D_i K_i^{\mathrm{L}} c_{i_o}}{\ell}\left\{1 - \exp\left[\frac{-\upsilon_i(\Delta p - \Delta\pi)}{RT}\right]\right\} \tag{2.41}$$

where Δp is the difference in hydrostatic pressure across the membrane ($p_o - p_\ell$). A trial calculation shows that the term $-\upsilon_i(\Delta p - \Delta\pi)/RT$ is small under the normal conditions of reverse osmosis. For example, in water desalination, when $\Delta p = 100$ atm, $\Delta\pi = 10$ atm, and $\upsilon_i = 18$ cm^3/mol, the term $\upsilon_i(\Delta p - \Delta\pi)/RT$ is about 0.06.

Under these conditions, the simplification $1 - \exp(x) \to x$ as $x \to 0$ can be used, and Equation (2.41) can be written to a very good approximation as

$$J_i = \frac{D_i K_i^{\mathrm{L}} c_{i_o} \upsilon_i(\Delta p - \Delta\pi)}{\ell RT} \tag{2.42}$$

This equation can be simplified to

$$J_i = A(\Delta p - \Delta\pi) \tag{2.43}$$

where A is a constant equal to the term $D_i K_i^{\mathrm{L}} c_{i_o} \upsilon_i/\ell RT$. In the reverse osmosis literature, the constant A is usually called the *water permeability constant*.

Similarly, a simplified expression for the salt flux, J_j, through the membrane can be derived, starting with the equivalent to Equation (2.37)

$$J_j = \frac{D_j K_j^{\mathrm{L}}}{\ell}\left\{c_{j_o} - c_{j_\ell}\exp\left[\frac{-\upsilon_j(p_o - p_\ell)}{RT}\right]\right\} \tag{2.44}$$

Because the term $-v_j(p_o - p_\ell)/RT$ is small, the exponential term in Equation (2.44) is close to one, and Equation (2.44) can then be written as

$$J_j = \frac{D_j K_j^{\mathrm{L}}}{\ell}(c_{j_o} - c_{j_\ell}) \tag{2.45}$$

or

$$J_j = B(c_{j_o} - c_{j_\ell}) \tag{2.46}$$

where B is usually called the *salt permeability constant* and has the value

$$B = \frac{D_j K_j^{\mathrm{L}}}{\ell} \tag{2.47}$$

Predictions of salt and water transport can be made from this application of the solution-diffusion model to reverse osmosis (first derived by Merten and coworkers) [12,13]. According to Equation (2.43), the water flux through a reverse osmosis membrane remains small up to the osmotic pressure of the salt solution and then increases with applied pressure, whereas according to Equation (2.46), the salt flux is essentially independent of pressure. Some typical results are shown in Figure 2.9. Also shown in this figure is a term called the rejection coefficient, $\mathbb{R}$, which is defined as

$$\mathbb{R} = \left(1 - \frac{c_{j_\ell}}{c_{j_o}}\right) \times 100\,\% \tag{2.48}$$

The rejection coefficient is a measure of the ability of the membrane to separate salt from the feed solution.

For a perfectly selective membrane the permeate salt concentration, $c_{j_\ell} = 0$ and $\mathbb{R} = 100\,\%$, and for a completely unselective membrane the permeate salt concentration is the same as the feed salt concentration, $c_{j_\ell} = c_{j_o}$ and $\mathbb{R} = 0\,\%$. The rejection coefficient increases with applied pressure as shown in Figure 2.9, because the water flux increases with pressure, but the salt flux does not.

Hyperfiltration

By convention, the term reverse osmosis is used to describe the separation of an aqueous salt solution by pressure-driven flow through a semipermeable membrane. Recently, the same type of process has been applied to the separation of organic mixtures. For example, Mobil Oil has installed a large plant to separate methyl ethyl ketone (MEK) from MEK–oil mixtures created in the production of lubricating oil [14] as described in Chapter 5. Separation of this type of mixture is probably best called hyperfiltration.

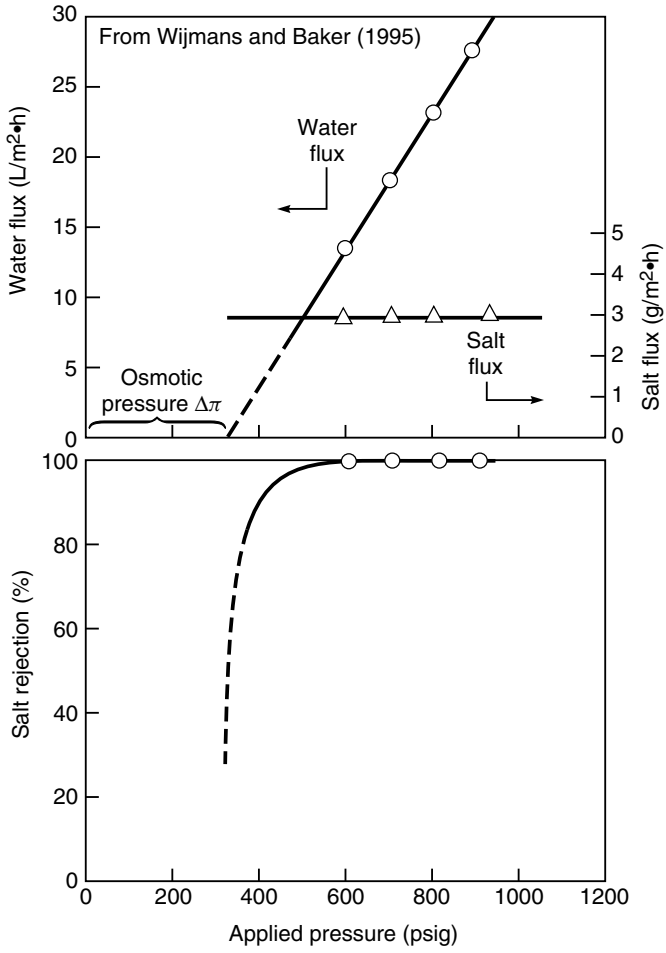

Figure 2.9 Flux and rejection data for a model seawater solution (3.5 % sodium chloride) in a good quality reverse osmosis membrane (FilmTec Corp. FT 30 membrane) as a function of pressure [10]. The salt flux, in accordance with Equation (2.44), is essentially constant and independent of pressure. The water flux, in accordance with Equation (2.43), increases with pressure, and, at zero flux, meets the pressure axis at the osmotic pressure of seawater ~350 psi

The mathematical description of this process is identical to that of reverse osmosis given in Equations (2.37) and (2.44) and leads to expressions for the solute and solvent fluxes

$$J_i = \frac{D_i K_i^{\mathrm{L}}}{\ell} \left\{ c_{i_o} - c_{i_\ell} \exp\left[\frac{-\upsilon_i (p_o - p_\ell)}{RT} \right] \right\} \tag{2.49}$$

and

$$J_j = \frac{D_j K_j^{\mathrm{L}}}{\ell}\left\{c_{j_o} - c_{j_\ell}\exp\left[\frac{-\upsilon_j(p_o - p_\ell)}{RT}\right]\right\} \tag{2.50}$$

With the advent of the personal computer, the numerical solution to these equations is straightforward even for multicomponent mixtures. Figure 2.10 shows an example calculation for the separation of a 20 wt% solution of *n*-decane in MEK. In these calculations, the ratio of the permeabilities of MEK

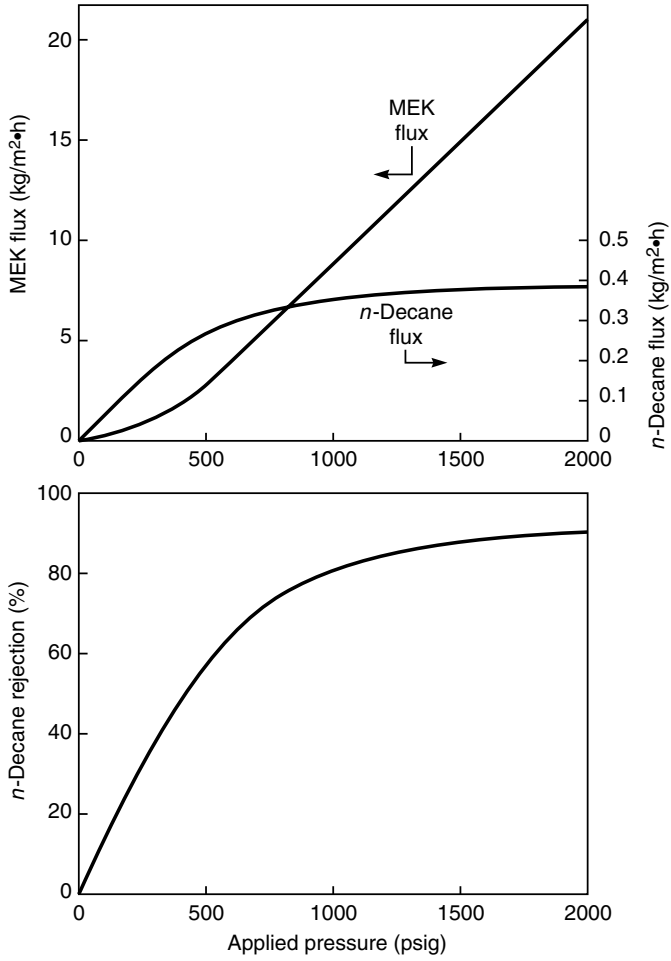

Figure 2.10 Flux and rejection curves calculated using Equations (2.49) and (2.50) for a 20 wt% *n*-decane solution in methyl ethyl ketone (MEK). MEK is assumed to be 10 times more permeable than *n*-decane

and n-decane, $D_i K_i / D_j K_j$, is set at 10. The curves have essentially the same form as the salt solution flux data in Figure 2.9. At high pressures, the rejection approaches a limiting value of 90 %, and the limiting Equations (2.43) for the solvent (MEK) flux and (2.47) for the solute flux apply.

Gas Separation

In gas separation, a gas mixture at a pressure p_o is applied to the feed side of the membrane, while the permeate gas at a lower pressure (p_ℓ) is removed from the downstream side of the membrane. As before, the starting point for the derivation of the gas separation transport equation is to equate the chemical potentials on either side of the gas/membrane interface. This time, however, the chemical potential for the gas phase is given by Equation (2.8) for a compressible fluid, whereas Equation (2.7) for an incompressible medium is applied to the membrane phase. Substitution of these equations into Equation (2.20) at the gas/membrane feed interface yields[3]

$$\mu_i^o + RT \ln(\gamma_{i_o}^{\mathrm{G}} n_{i_o}) + RT \ln \frac{p_o}{p_{i_{\mathrm{sat}}}} = \mu_i^o + RT \ln(\gamma_{i_{o(m)}} n_{i_{o(m)}}) + \upsilon_i (p_o - p_{i_{\mathrm{sat}}}) \tag{2.51}$$

which rearranges to

$$n_{i_{o(m)}} = \frac{\gamma_{i_o}^{\mathrm{G}}}{\gamma_{i_{o(m)}}} \cdot \frac{p_o}{p_{i_{\mathrm{sat}}}} \cdot n_{i_o} \exp\left[\frac{-\upsilon_i (p_o - p_{i_{\mathrm{sat}}})}{RT}\right] \tag{2.52}$$

Because the exponential term is again very close to one,[4] even for very high pressures (p_o), Equation (2.52) reduces to

$$n_{i_{o(m)}} = \frac{\gamma_{i_o}^{\mathrm{G}} n_{i_o}}{\gamma_{i_{o(m)}}} \cdot \frac{p_o}{p_{i_{\mathrm{sat}}}} \tag{2.53}$$

The term $n_{i_o} p_o$ is the partial pressure of i in the feed gas, p_{i_o}. Equation (2.53) then simplifies to

$$n_{i_{o(m)}} = \frac{\gamma_{i_{(o)}}^{\mathrm{G}}}{\gamma_{i_{o(m)}}} \cdot \frac{p_{i_o}}{p_{i_{\mathrm{sat}}}} \tag{2.54}$$

or

$$c_{i_{o(m)}} = m_i \rho_m \frac{\gamma_{i_o}^{\mathrm{G}} p_{i_o}}{\gamma_{i_{o(m)}} p_{i_{\mathrm{sat}}}} \tag{2.55}$$

[3] At this point the superscript G is introduced to denote the gas phase. For example γ_i^{G}, the activity of component i in the gas phase, and K_i^{G}, the sorption coefficient of component i between the gas and membrane phases [Equation (2.56)].

[4] In evaluating this exponential term (the Poynting correction), it is important to recognize that υ_i is not the molar volume of i in the gas phase, but the molar volume of i dissolved in the membrane material, which is approximately equal to the molar volume of liquid i.

By defining a gas phase sorption coefficient K_i^{G} as

$$K_i^{\mathrm{G}} = \frac{m_i \rho_m \gamma_{i_o}^{\mathrm{G}}}{\gamma_{i_{o(m)}} p_{i_{\mathrm{sat}}}} \tag{2.56}$$

the concentration of component i at the feed interface of the membrane can be written as

$$c_{i_{o(m)}} = K_i^{\mathrm{G}} \cdot p_{i_o} \tag{2.57}$$

In exactly the same way, the concentration of component i at the membrane/permeate interface can be shown to be

$$c_{i_{\ell(m)}} = K_i^{\mathrm{G}} \cdot p_{i_\ell} \tag{2.58}$$

Combining Equations (2.57) and (2.58) with the Fick's law expression, Equation (2.13), gives

$$J_i = \frac{D_i K_i^{\mathrm{G}} (p_{i_o} - p_{i_\ell})}{\ell} \tag{2.59}$$

The product $D_i K_i^{\mathrm{G}}$ is often abbreviated to a permeability coefficient, P_i^{G}, to give the familiar expression

$$J_i = \frac{P_i^{\mathrm{G}} (p_{i_o} - p_{i_\ell})}{\ell} \tag{2.60}$$

Equation (2.60) is widely used to accurately and predictably rationalize the properties of gas permeation membranes.

The derivation of Equation (2.60) might be seen as a long-winded way of arriving at a trivial result. However, this derivation explicitly clarifies the assumptions behind this equation. First, a gradient in concentration occurs within the membrane, but there is no gradient in pressure. Second, the absorption of a component into the membrane is proportional to its activity (partial pressure) in the adjacent gas, but is independent of the total gas pressure. This is related to the approximation made in Equation (2.52), in which the Poynting correction was assumed to be 1.

The permeability coefficient, P_i^{G}, equal to the product $D_i K_i^{\mathrm{G}}$ can be expressed from the definition of K_i^{G} in Equation (2.56) as

$$P_i^{\mathrm{G}} = \frac{\gamma_i^{\mathrm{G}} D_i m_i \rho_m}{\gamma_{i_{(m)}} \cdot p_{i_{\mathrm{sat}}}} \tag{2.61}$$

In Equation (2.60) the membrane flux, J_i, is a mass flux (g/cm$^2 \cdot$ s), whereas the gas separation literature predominantly uses a molar flux, typically expressed in the units cm^3(STP)/cm$^2 \cdot$ s. The molar flux, j_i, can be linked to the mass flux, J_i, by the expression

$$j_i = J_i \frac{\upsilon_i^{\mathrm{G}}}{m_i} \tag{2.62}$$

where υ_i^G is the molar volume of gas i (cm^3(STP)/mol). Similarly the mass permeability unit P_i^G, defined in Equation (2.60), can be linked to the molar gas permeability $\mathcal{P}_i^G$, usually in the units $cm^3(STP) \cdot cm/cm^2 \cdot s \cdot cmHg$, as

$$\mathcal{P}_i^G = \frac{P_i^G \upsilon_i^G}{m_i} \tag{2.63}$$

Equation (2.60) can then be written as

$$j_i = \frac{\mathcal{P}_i^G}{\ell}(p_{i_o} - p_{i_\ell}) \tag{2.64}$$

and combining Equations (2.61) and (2.63) gives

$$\mathcal{P}_i^G = \frac{\gamma_i^G D_i \upsilon_i^G \rho_{(m)}}{\gamma_{i_{(m)}} p_{i_{sat}}} \tag{2.65}$$

Equation (2.65) is not commonly used as an expression for gas-phase membrane permeability, but is of interest because it shows that large permeability coefficients are obtained for compounds with a large diffusion coefficient (D_i), a limited affinity for the gas phase (large γ_i^G), a high affinity for the membrane material (small $\gamma_{i(m)}$), and a low saturation vapor pressure ($p_{i_{sat}}$). The molar gas permeation permeability ($\mathcal{P}_i^G$) is close to being a materials constant, relatively independent of the composition and pressure of the feed and permeate gases. This is in sharp contrast to the permeability constant for liquids as described in the discussion centered on Figure 2.7 earlier, but, even for gases, the concept of permeability as a materials constant must be treated with caution. For example, the permeability of vapors at partial pressures close to saturation often increases substantially with increasing partial pressure. This effect is commonly ascribed to plasticization and other effects of the permeant on the membrane, changing D_i and $\gamma_{i_{(m)}}$ in Equation (2.65). However, significant deviations of the vapor's activity coefficient, γ_i^G, from ideality can also occur at high partial pressures.

Equation (2.65) is also a useful way to rationalize the effect of molecular weight on permeability. The permeant's saturation vapor pressure ($p_{i_{sat}}$) and diffusion coefficient both decrease with increasing molecular weight, creating competing effects on the permeability coefficient. In glassy polymers, the decrease in diffusion coefficient far outweighs other effects, and permeabilities fall significantly as molecular weight increases [15]. In rubbery polymers, on the other hand, the two effects are more balanced. For molecular weights up to 100, permeability generally increases with increasing molecular weight because $p_{i_{sat}}$ is the dominant term. Above molecular weight 100, the molecular weight term gradually becomes dominant, and permeabilities fall with increasing molecular weight of the permeant. Some data illustrating this behavior for permeation of simple alkanes in silicone rubber membranes are shown in Figure 2.11. As the molecular weight increases from CH_4 to C_5H_{12}, the effect of the decrease in $p_{i_{sat}}$

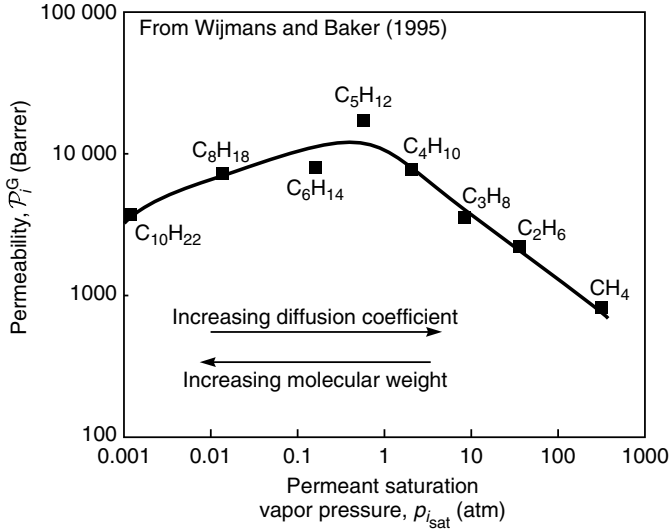

Figure 2.11 Permeability coefficient, $\mathcal{P}_i^{\mathrm{G}}$, of n-alkanes in poly(dimethylsiloxane) as a function of saturation pressure ($p_{i_{\mathrm{sat}}}$)

is larger than the effect of increasing size or D_i. Above pentane, however, the trend is reversed.

Pervaporation

Pervaporation is a separation process in which a multicomponent liquid is passed across a membrane that preferentially permeates one or more of the components. A partial vacuum is maintained on the permeate side of the membrane, so that the permeating components are removed as a vapor mixture. Transport through the membrane is induced by maintaining the vapor pressure of the gas on the permeate side of the membrane at a lower vapor pressure than the feed liquid. The gradients in chemical potential, pressure, and activity across the membrane are illustrated in Figure 2.12.

At the liquid solution/membrane feed interface, the chemical potential of the feed liquid is equilibrated with the chemical potential in the membrane at the same pressure. Equation (2.7) then gives

$$\mu_i^o + RT\ln(\gamma_{i_o}^{\mathrm{L}} n_{i_o}) + \upsilon_i(p_o - p_{i_{\mathrm{sat}}}) = \mu_i^o + RT\ln(\gamma_{i_{o(m)}} n_{i_{o(m)}}) + \upsilon_i(p_o - p_{i_{\mathrm{sat}}}) \tag{2.66}$$

which leads to an expression for the concentration at the feed side interface

$$c_{i_{o(m)}} = \frac{\gamma_{i_o}^{\mathrm{L}}\rho_m}{\gamma_{i_{o(m)}}\rho_o} \cdot c_{i_o} = K_i^{\mathrm{L}} \cdot c_{i_o} \tag{2.67}$$

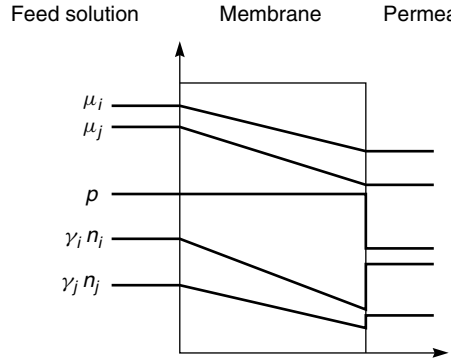

Figure 2.12 Chemical potential, pressure, and activity profiles through a pervaporation membrane following the solution-diffusion model

where K_i^{L} is the liquid-phase sorption coefficient defined in Equation (2.26) in the dialysis section.

At the permeate gas/membrane interface, the pressure drops from p_o in the membrane to p_ℓ in the permeate vapor. The equivalent expression for the chemical potentials in each phase is then

$$\mu_i^o + RT\ln(\gamma_{i_\ell}^{\mathrm{G}} n_{i_\ell}) + RT\ln\left(\frac{p_\ell}{p_{i_{\mathrm{sat}}}}\right) = \mu_i^o + RT\ln(\gamma_{i_{\ell(m)}} n_i) + \upsilon_i(p_o - p_{i_{\mathrm{sat}}}) \tag{2.68}$$

Rearranging Equation (2.68) gives

$$n_{i_{\ell(m)}} = \frac{\gamma_{i_\ell}^{\mathrm{G}}}{\gamma_{i_{\ell(m)}}} \cdot \frac{p_\ell}{p_{i_{\mathrm{sat}}}} \cdot n_{i_\ell} \cdot \exp\left[\frac{-\upsilon_i(p_o - p_{i_{\mathrm{sat}}})}{RT}\right] \tag{2.69}$$

As before, the exponential term is close to unity; thus, the concentration at the permeate side interface is

$$n_{i_{\ell(m)}} = \frac{\gamma_{i_\ell}^{\mathrm{G}}}{\gamma_{i_{\ell(m)}}} \cdot n_{i_\ell} \cdot \frac{p_\ell}{p_{i_{\mathrm{sat}}}} \tag{2.70}$$

The product $n_{i_\ell} p_\ell$ can be replaced by the partial pressure term p_{i_ℓ}, thus

$$n_{i_{\ell(m)}} = \frac{\gamma_{i_\ell}^{\mathrm{G}}}{\gamma_{i_{\ell(m)}}} \cdot \frac{p_{i_\ell}}{p_{i_{\mathrm{sat}}}} \tag{2.71}$$

or, substituting concentration for mole fraction from Equation (2.10),

$$c_{i_{\ell(m)}} = m_i \rho_m \cdot \frac{\gamma_{i_\ell}^{\mathrm{G}} p_{i_\ell}}{\gamma_{i_{\ell(m)}} p_{i_{\mathrm{sat}}}} = K_i^{\mathrm{G}} p_{i_\ell} \tag{2.72}$$

where K_i^{G} is the gas-phase sorption coefficient defined in Equation (2.56) in the gas separation section.

The concentration terms in Equations (2.67) and (2.72) can be substituted into Equation (2.13) (Fick's law) to obtain an expression for the membrane flux.

$$J_i = \frac{D_i(K_i^{\mathrm{L}} c_{i_o} - K_i^{\mathrm{G}} p_{i_\ell})}{\ell} \tag{2.73}$$

However, the sorption coefficient in Equation (2.67) is a liquid-phase coefficient, whereas the sorption coefficient in Equation (2.72) is a gas-phase coefficient. The interconversion of these two coefficients can be handled by considering a hypothetical vapor in equilibrium with a feed solution. This vapor–liquid equilibrium can then be written

$$\mu_i^o + RT\ln(\gamma_i^{\mathrm{L}} n_i^{\mathrm{L}}) + \upsilon_i(p - p_{i_{\mathrm{sat}}}) = \mu_i^o + RT\ln(\gamma_i^{\mathrm{G}} n_i^{\mathrm{G}}) + RT\ln\left(\frac{p}{p_{i_{\mathrm{sat}}}}\right) \tag{2.74}$$

where the superscripts L and G represent the liquid and the gas phases. By following the same steps as were taken from Equation (2.68) to (2.72), Equation (2.74) becomes

$$n_i^{\mathrm{L}} = \frac{\gamma_i^{\mathrm{G}} p_i}{\gamma_i^{\mathrm{L}} p_{i_{\mathrm{sat}}}} \tag{2.75}$$

Substituting for concentration with Equation (2.10) gives

$$c_i^{\mathrm{L}} = m_i \rho \frac{\gamma_i^{\mathrm{G}} p_i}{\gamma_i^{\mathrm{L}} p_{i_{\mathrm{sat}}}} \tag{2.76}$$

and so

$$c_i^{\mathrm{L}} = \frac{K_i^{\mathrm{G}}}{K_i^{\mathrm{L}}} \cdot p_i \tag{2.77}$$

This expression links the concentration of component i in the liquid phase, c_i^{L} with p_i, the partial vapor pressure of i in equilibrium with the liquid. Substitution of Equation (2.77) into Equation (2.73) yields

$$J_i = \frac{D_i K_i^{\mathrm{G}}(p_{i_o} - p_{i_\ell})}{\ell} \tag{2.78}$$

where p_{i_o} and p_{i_ℓ} are the partial vapor pressures of component i on either side of the membrane. Equation (2.67) can also be written as

$$J_i = \frac{P_i^{\mathrm{G}}}{\ell}(p_{i_o} - p_{i_\ell}) \tag{2.79}$$

This equation explicitly expresses the driving force in pervaporation as the vapor pressure difference across the membrane, a form of the pervaporation process

derived first by Kataoka *et al.* [16]. Equation (2.77) links the concentration of a sorbed vapor in the liquid phase ($c_{i_o}^{\mathrm{L}}$) with the equilibrium partial pressure of the vapor. This is known as Henry's law and is usually written as[5]

$$H_i \cdot c_i^{\mathrm{L}} = p_i \tag{2.80}$$

From Equations (2.77) and (2.80) it follows that the Henry's law coefficient, H_i, can be written as

$$H_i = \frac{K_i^{\mathrm{L}}}{K_i^{\mathrm{G}}} = \frac{\gamma_i^{\mathrm{L}} p_{i_{\mathrm{sat}}}}{m_i \rho \gamma_i^{\mathrm{G}}} \tag{2.81}$$

These expressions can be used to write Equation (2.73) as

$$J_i = \frac{P_i^{\mathrm{G}}}{\ell}(c_{i_o} H_i - p_{i_\ell}) \tag{2.82}$$

or

$$J_i = \frac{P_i^{\mathrm{L}}}{\ell}(c_{i_o} - p_{i_\ell}/H_i) \tag{2.83}$$

Equation (2.79) expresses the driving force in pervaporation in terms of the vapor pressure. The driving force could equally well have been expressed in terms of concentration differences, as in Equation (2.83). However, in practice, the vapor pressure expression provides much more useful results and clearly shows the connection between pervaporation and gas separation, Equation (2.60). Also, P_i^{G}, the gas phase coefficient, is much less dependent on temperature than P_i^{L}. The reliability of Equation (2.79) has been amply demonstrated experimentally [17,18]. Figure 2.13, for example, shows data for the pervaporation of water as a function of permeate pressure. As the permeate pressure (p_{i_ℓ}) increases, the water flux falls, reaching zero flux when the permeate pressure is equal to the feed-liquid vapor pressure ($p_{i_{\mathrm{sat}}}$) at the temperature of the experiment. The straight lines in Figure 2.13 indicate that the permeability coefficient (P_i^{G}) of water in silicone rubber is constant, as expected in this and similar systems in which the membrane material is a rubbery polymer and the permeant swells the polymer only moderately.

Greenlaw *et al.* [18] have studied the effect of feed and permeate pressure on pervaporation flux in some detail; some illustrative results are shown in

[5]In Equation (2.80), the Henry's law coefficient H_i has the units atm $\cdot$ cm^3/g. More commonly, Henry's law is written in terms of mole fraction:

$$H_i' \cdot n_i^{\mathrm{L}} = p_i$$

where H_i' has the units atm/mol fraction. Using Equation (2.10), the two coefficients are linked by the expression

$$H_i = \frac{H_i'}{m_i \cdot p_i}$$

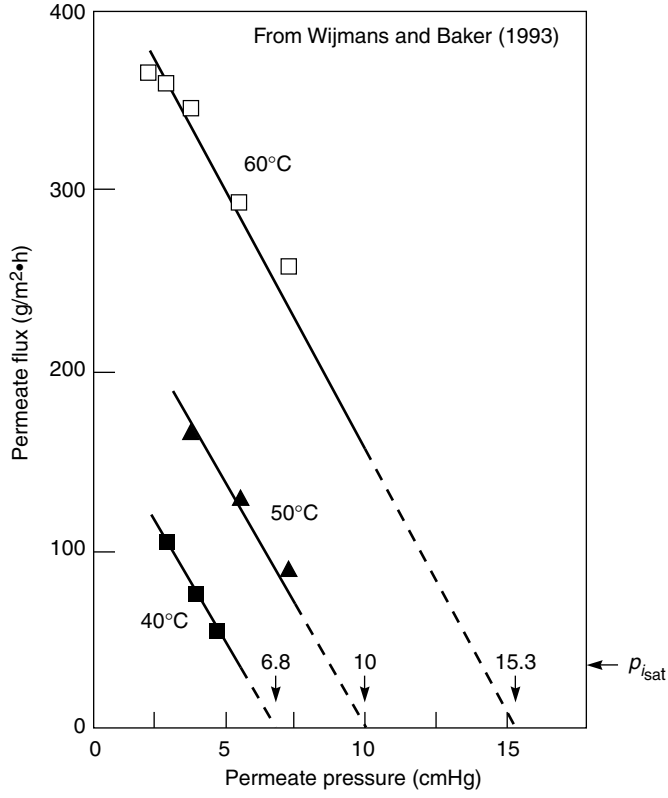

Figure 2.13 The effect of permeate pressure on the water flux through a silicone rubber pervaporation membrane. The arrows on the lower axis represent the saturation vapor pressures of the feed solution at the temperature of these experiments as predicted by Equation (2.79) [15]

Figure 2.14. As Figure 2.14(a) shows, the dependence of flux on permeate pressure in pervaporation is in accordance with Equation (2.79). The flux decreases with increasing permeate pressure, reaching a minimum value when the permeate pressure equals the saturation vapor pressure of the feed. The curvature of the line in Figure 2.14(a) shows that the permeability coefficient decreases with decreasing permeate pressure, that is, P^{G}_{hexane} decreases as hexane concentration in the membrane decreases. This behavior is typical of membranes that are swollen significantly by the permeant. If, on the other hand, as shown in Figure 2.14(b), the permeate pressure is fixed at a low value, the hydrostatic pressure of the feed liquid can be increased to as much as 20 atm without any significant change in the flux. This is because increased hydrostatic pressure produces a minimal change in the partial pressure of the feed liquid partial pressure (p_{i_o}), the true

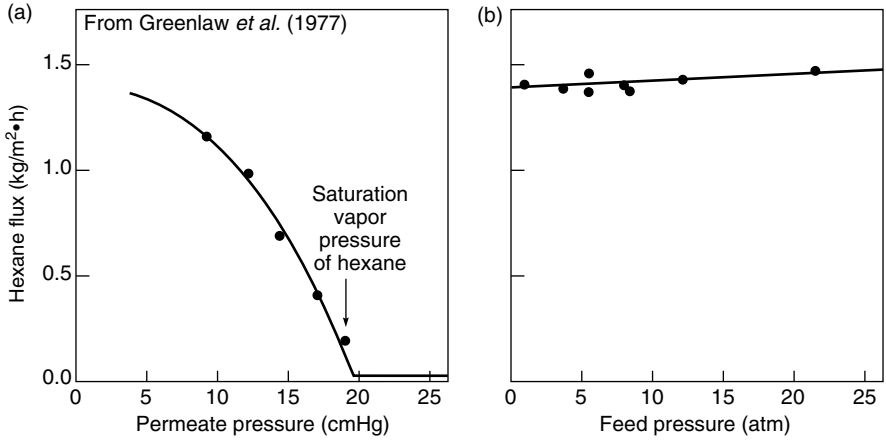

Figure 2.14 The effect of feed and permeate pressure on the flux of hexane through a rubbery pervaporation membrane. The flux is essentially independent of feed pressure up to 20 atm but is extremely sensitive to permeate pressure [18]. The explanation for this behavior is in the transport equation (2.79). Reprinted from *J. Membr. Sci.* **2**, F.W. Greenlaw, W.D. Prince, R.A. Shelden and E.V. Thompson, Dependence of Diffusive Permeation Rates by Upstream and Downstream Pressures, p. 141, Copyright 1977, with permission from Elsevier

driving force shown in Equation (2.79). Thus, the properties of pervaporation membranes illustrated in Figures 2.13 and 2.14 are easily rationalized by the solution-diffusion model but are much more difficult to explain by a pore-flow mechanism, although this has been tried.

Evidence for the Solution-diffusion Model

In the discussion above, the solution-diffusion model was used to derive equations that predict the experimentally observed performance of the membrane processes of dialysis, gas separation, reverse osmosis, and pervaporation. It was not necessary to resort to any additional process-specific model to obtain these results. This agreement between theory and experiment is good evidence for the validity of the solution-diffusion model. Moreover, the large body of permeability, diffusion, and partition coefficient data obtained over the past 20 years for these membrane processes are in good numerical agreement with one another. This universality and the simplicity of the solution-diffusion model are its most useful features and are a strong argument for the validity of the model. Finally, a number of direct experimental measurements can be made to distinguish between the solution-diffusion model and other models, such as the pore-flow model.

One prediction of the solution-diffusion model, controversial during the 1970s, is that the action of an applied pressure on the feed side of the membrane is to

decrease the concentration of the permeant on the low pressure side of the membrane. This counterintuitive effect is illustrated by Figures 2.5 and 2.6. A number of workers have verified this prediction experimentally with a variety of polymer membranes, ranging from diffusion of water in glassy cellulose acetate membranes to diffusion of organics in swollen rubbers [19–21]. Convincing examples of this type of experiment are the results of Rosenbaum and Cotton shown in Figure 2.15 [20]. In these experiments, four thin cellulose acetate films were laminated together, placed in a high pressure reverse osmosis cell, and subjected

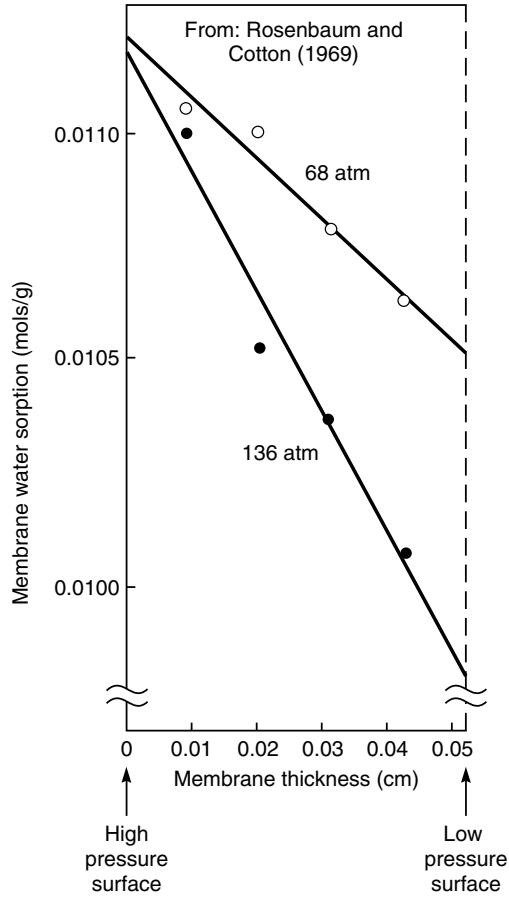

Figure 2.15 Measurements of Rosenbaum and Cotton [20] of the water concentration gradients in a laminated reverse osmosis cellulose acetate membrane under applied pressures of 68 and 136 atm. Reprinted from Steady-state Distribution of Water in Cellulose Acetate Membrane, S. Rosenbaum and O. Cotton, *J. Polym. Sci.* **7**, 101; Copyright © 1969. This material is used by permission of John Wiley & Sons, Inc.

to feed pressures of 68 or 136 atm. The permeate was maintained at atmospheric pressure. After permeation through the membrane laminate had reached a steady state, the membrane was quickly removed from the cell, and the water concentration in each laminate measured. As predicted by the solution-diffusion model and shown in Figure 2.15, the applied pressure decreases the concentration of water on the permeate side of the membrane. Also, the concentration difference across the membrane at 136 atm applied pressure is about twice that observed at 68 atm, and the measured concentration on the permeate side is within 20 % of the expected value calculated from Equation (2.36).

Another series of papers by Paul and co-workers [4–6,19,22] focuses on the same phenomenon using rubbery membranes and permeation of organic solvents such as hexane, benzene and carbon tetrachloride. Such membranes are highly swollen by the organic solvents and, when operated in reverse osmosis mode,

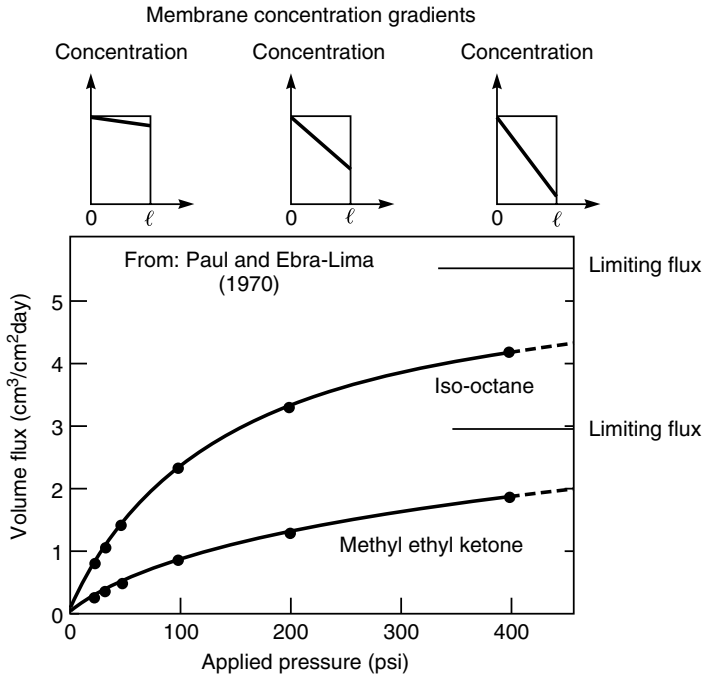

Figure 2.16 Pressure permeation (reverse osmosis) of iso-octane and methyl ethyl ketone through crosslinked 265-μm-thick natural rubber membranes. The change in the concentration gradient in the membrane as the applied pressure is increased is illustrated by the inserts. At high applied pressures, the concentration gradient and the permeation fluxes approach their limiting values [4]. Reprinted from Pressure-induced Diffusion of Organic Liquids Through Highly Swollen Polymer Membranes," D.R. Paul and O.M. Ebra-Lima, *J. Appl. Polym. Sci.* **14**, 2201; Copyright © 1970. This material is used by permission of John Wiley & Sons, Inc.

large concentration gradients develop through the membrane even at relatively modest applied pressures. This means that the concentration in the membrane on the permeate side approaches zero and the flux through the membrane reaches a limiting value as the feed pressure is increased. Representative data are shown in Figure 2.16.

Paul and Paciotti [19] took this work a step further by measuring the flux of a liquid (hexane) through a membrane both in pervaporation experiments with atmospheric pressure on the feed side of the membrane and a vacuum on the permeate side, and in reverse osmosis experiments with liquid at elevated pressures on the feed side and at atmospheric pressure on the permeate side. The hexane flux obtained in these two sets of experiments is plotted in Figure 2.17 against the hexane concentration difference in the membrane ($c_{i_{o(m)}} - c_{i_{\ell(m)}}$). The concentrations, $c_{i_{o(m)}}$ and $c_{i_{\ell(m)}}$, were calculated from Equations (2.26), (2.36) and (2.72).

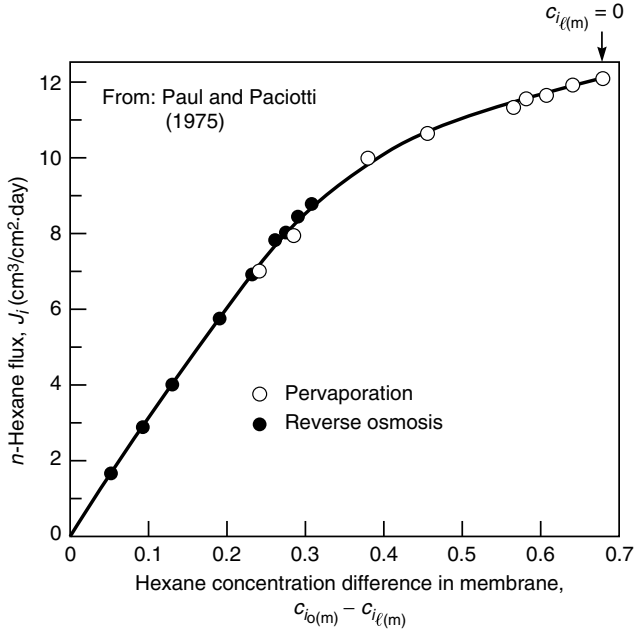

Figure 2.17 Flux of *n*-hexane through a rubbery membrane as a function of the hexane concentration difference in the membrane. Data taken from both reverse osmosis (●) and pervaporation (○) experiments. Feed-side and permeate-side membrane concentrations, $c_{i_{o(m)}}$ and $c_{i_{\ell(m)}}$, calculated from the operating conditions through Equations (2.26), (2.36) and (2.76). Maximum flux is obtained at the maximum concentration difference, when the permeate-side membrane concentration ($c_{i_{\ell(m)}}$), equals zero [19]. Reprinted from Driving Force for Hydraulic and Pervaporation Transport in Homogeneous Membranes, D.R. Paul and D.J. Paciotti, *J. Polym. Sci., Polym. Phys. Ed.* **13**, 1201; Copyright © 1975. This material is used by permission of John Wiley & Sons, Inc.

Sorption data were used to obtain values for K_i^L. As pointed out by Paul and Paciotti, the data in Figure 2.17 show that reverse osmosis and pervaporation obey one unique transport equation—Fick's law. In other words, transport follows the solution-diffusion model. The slope of the curve decreases at the higher concentration differences, that is, at smaller values for $c_{i_{\ell(m)}}$ because of decreases in the diffusion coefficient, as the swelling of the membrane decreases.

The results illustrated in Figure 2.16 show that the solvent flux tends towards a limiting value at very high pressures. This value is reached when the concentration of sorbed solvent at the permeate side of the membrane reaches zero, the limiting value.

Structure–Permeability Relationships in Solution-diffusion Membranes

In the preceding section the effect of concentration and pressure gradient driving forces on permeation through membranes was described in terms of the solution-diffusion model and Fick's law. The resulting equations all contain a permeability term, P, that must be experimentally determined. This section describes how the nature of the membrane material affects permeant diffusion and sorption coefficients, which in turn determine membrane permeability. This is a difficult subject. By analyzing the factors that determine membrane permeability, useful correlations and rules of thumb can be derived to guide the selection of membrane materials with the optimum flux and selectivity properties. Most of the experimental data in this area have been obtained with gas-permeable membranes. However, the same general principles apply to all polymeric solution-diffusion membranes.

The problem of predicting membrane permeability can be divided into two parts because permeability is the product of the diffusion coefficient and the sorption coefficient:

$$P = D \cdot K \tag{2.84}$$

The sorption coefficient (K) in Equation (2.84) is the term linking the concentration of a component in the fluid phase with its concentration in the membrane polymer phase. Because sorption is an equilibrium term, conventional thermodynamics can be used to calculate solubilities of gases in polymers to within a factor of two or three. However, diffusion coefficients (D) are kinetic terms that reflect the effect of the surrounding environment on the molecular motion of permeating components. Calculation of diffusion coefficients in liquids and gases is possible, but calculation of diffusion coefficients in polymers is much more difficult. In the long term, the best hope for accurate predictions of diffusion in polymers is the molecular dynamics calculations described in an earlier section. However, this technique is still under development and is currently limited to calculations of the diffusion of small gas molecules in amorphous polymers; the

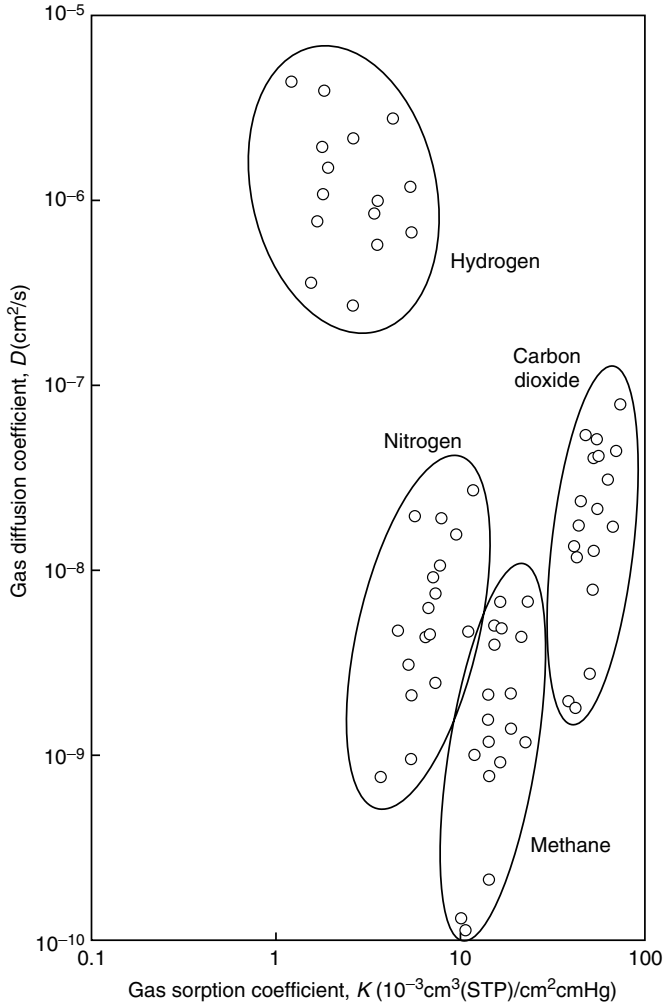

Figure 2.18 Diffusion and sorption coefficients plotted for gases in a family of 18 related polyimides. Data of Tanaka *et al*. [23]

agreement between theory and experiment is modest. In the meantime, simple correlations based on polymer free volume must be used.

As a general rule, membrane material changes affect the diffusion coefficient of a permeant much more than the sorption coefficient. For example, Figure 2.18 shows some typical gas permeation data taken from a paper of Tanaka *et al*. [23]. The diffusion and sorption coefficients of four gases in a family of 18 related polyimides are plotted against each other. Both sorption and diffusion coefficients

are fairly well grouped for each gas. However, for any one gas the difference in diffusion coefficient from the highest to lowest value is approximately 100-fold, whereas the spread in sorption coefficient is only 2- to 4-fold. Changes in polymer chemistry affect both the sorption and diffusion coefficients, but the effect on the diffusion coefficient is much more profound.

More detailed examination of the data shown in Figure 2.18 shows that the relative position of each polymer within the group of 18 is approximately the same for all gases. That is, the polymer with the highest diffusion coefficient for methane also has the highest diffusion coefficient for nitrogen, carbon dioxide and hydrogen. The trend for the solubility coefficients is similar. As a general rule, changes in polymer chemistry and structure that change the diffusion coefficient or sorption coefficient of one gas change the properties of other gases in the same way. This is why membrane permeabilities can be easily varied by orders of magnitude by changing the membrane material, whereas changing membrane selectivities (proportional to the ratio of permeabilities) by more than a factor of two or three is difficult.

In the following sections the factors that determine the magnitude of diffusion and solubility coefficients in polymers are discussed.

Diffusion Coefficients

The Fick's law diffusion coefficient of a permeating molecule is a measure of the frequency with which the molecule moves and the size of each movement. Therefore, the magnitude of the diffusion coefficient is governed by the restraining forces of the medium on the diffusing species. Isotopically labeled carbon in a diamond lattice has a very small diffusion coefficient. The carbon atoms of diamond move infrequently, and each movement is very small—only 1 to 2 Å. On the other hand, isotopically labeled carbon dioxide in a gas has an extremely large diffusion coefficient. The gas molecules are in constant motion and each jump is of the order of 1000 Å or more. Table 2.1 lists some representative values of diffusion coefficients in different media.

Table 2.1 Typical diffusion coefficients in various media (25 °C)

Permeant/material	Diffusion coefficient, D (cm^2/s)
Oxygen in air (atmospheric pressure)	1×10^{-1}
Salt in water	1.5×10^{-5}
Albumin (MW 60 000) in water	6×10^{-7}
Oxygen in silicone rubber	1×10^{-5}
Oxygen in polysulfone	4×10^{-8}
Sodium atoms in sodium chloride crystals	1×10^{-20}
Aluminum atoms in metallic copper	1×10^{-30}

The main observation from Table 2.1 is the enormous range of values of diffusion coefficients—from 10^{-1} to 10^{-30} cm^2/s. Diffusion in gases is well understood and is treated in standard textbooks dealing with the kinetic theory of gases [24,25]. Diffusion in metals and crystals is a topic of considerable interest to the semiconductor industry but not to membrane permeation. This book focuses principally on diffusion in liquids and polymers in which the diffusion coefficient can vary from about 10^{-5} to about 10^{-10} cm^2/s.

Diffusion in Liquids

Liquids are simple, well defined systems and provide the starting point for modern theories of diffusion. An early and still fundamentally sound equation was derived by Einstein who applied simple macroscopic hydrodynamics to diffusion at the molecular level. He assumed the diffusing solute to be a sphere moving in a continuous fluid of solvent, in which case it can be shown that

$$D = \frac{kT}{6\pi a\eta} \tag{2.85}$$

where k is Boltzmann's constant, a is the radius of the solute and η is the solution viscosity. This is known as the Stokes–Einstein equation. The equation is a good approximation for large solutes with radii greater than 5–10 Å. But, as the solute becomes smaller, the approximation of the solvent as a continuous fluid becomes less valid. In this case there may be slip of solvent at the solute molecule's surface. A second limiting case assumes complete slip at the surface of the solute sphere; in this case

$$D = \frac{kT}{4\pi a\eta} \tag{2.86}$$

Thus, the Stokes–Einstein equation is perhaps best expressed as

$$D = \frac{kT}{n\pi a\eta} \qquad 4 \leq n \leq 6 \tag{2.87}$$

An important conclusion to be drawn from the Stokes–Einstein equation is that the diffusion coefficient of solutes in a liquid only changes slowly with molecular weight, because the diffusion coefficient is proportional to the reciprocal of the radius, which in turn is approximately proportional to the cube root of the molecular weight.

Application of the Stokes–Einstein equation requires a value for the solute radius. A simple approach is to assume the molecule to be spherical and to calculate the solute radius from the molar volume of the chemical groups making up the molecule. Using values for the solute radius calculated this way along with measured and known diffusion coefficients of solutes in water, Edward [26]

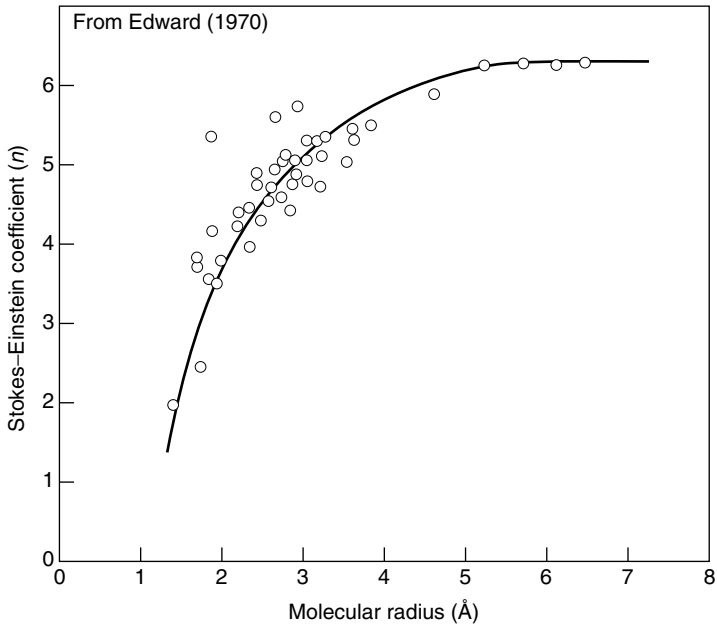

Figure 2.19 Value of the coefficient n in the Stokes–Einstein equation [Equation (2.87)] required to achieve agreement between calculation and experimental solute diffusion coefficients in water. [26]. Reprinted with permission from the *Journal of Chemical Education* **47**, No. 4, 1970, pp. 261–270, Figure 12, copyright © 1970, Division of Chemical Education, Inc.

constructed the graph of the coefficient n in the Stokes–Einstein equation, Equation (2.87), as a function of solute radius as shown in Figure 2.19. With large solutes, n approaches 6, that is, Einstein's application of normal macroscopic fluid dynamics at the molecular level is a valid approximation. However, when the solute radius falls below about 4 Å water can no longer be regarded as a continuous fluid, and n falls below 6. Nonetheless, that an equation based on macroscopic hydrodynamic theory applies to molecules to the 4 Å level is an interesting result.

The Stokes–Einstein equation works well for diffusion of solutes in simple liquids but fails in more complex fluids, such as a solution of a high-molecular-weight polymer. Dissolving a polymer in a liquid increases the solvent's viscosity, but the solute's diffusion coefficient is not significantly affected. For example, as the concentration of poly(vinyl pyrrolidone) dissolved in water is changed from 0 to 20 wt %, the viscosity of the solution increases by several orders of magnitude. However, the diffusion coefficient of sucrose in these solutions only changes by a factor of four [27]. The long polymer chains of dissolved poly(vinyl pyrrolidone) molecules link distant parts of the aqueous solution and change the viscosity of the

fluid substantially, but, in the fluid immediately surrounding the diffusing sucrose molecule, the effect of polymer chain length is much less noticeable. This result illustrates the difference between the microscopic viscosity in the immediate environment of the diffusing solute and the macroscopic viscosity measured by conventional viscometers. In simple liquids the macroscopic and microscopic viscosities are the same, but in liquids containing dissolved macromolecules, or in gels and polymer films, the microscopic viscosity and the macroscopic viscosity differ significantly.

Diffusion in Polymers

The concept that the local environment around the permeating molecule determines the permeate's diffusion coefficient is key to understanding diffusion in polymer membranes. Polymers can be divided into two broad categories—rubbery and glassy. In a rubbery polymer, segments of the polymer backbone can rotate freely around their axis; this makes the polymer soft and elastic. Thermal motion of these segments also leads to high permeant diffusion coefficients. In a glassy polymer, steric hindrance along the polymer backbone prohibits rotation of polymer segments; the result is a rigid, tough polymer. Thermal motion in this type of material is limited, so permeant diffusion coefficients are low. If the temperature of a glassy polymer is raised, a point is reached at which the increase in thermal energy is sufficient to overcome the steric hindrance restricting rotation of polymer backbone segments. At this temperature, called the *glass transition temperature* (T_g), the polymer changes from a glass to a rubber.

Figure 2.20 shows a plot of diffusion coefficient as a function of molecular weight for permeants diffusing through a liquid (water), two soft rubbery polymers (natural rubber and silicone rubber), and a hard, stiff glassy polymer (polystyrene) [28]. For very small molecules, such as helium and hydrogen, the diffusion coefficients in all of the media are comparable, differing by no more than a factor of two or three. These very small molecules only interact with one or two atoms in their immediate proximity. The local environment for these small solutes in the three polymers is not radically different to that in a liquid such as water. On the other hand, larger diffusing solutes with molecular weights of 200 to 300 and above have molecular diameters of 6 to 10 Å. Such solutes are in quite different local environments in the different media. In water, the Stokes–Einstein equation applies, and the resistance to movement of the solute is not much larger than that of a very small solute. In polymer membranes, however, several segments of the polymer chain are involved in each movement of the diffusing species. This type of cooperative movement is statistically unlikely; consequently, diffusion coefficients are much smaller than in liquid water. Moreover, the differences between the motion of polymer segments in the flexible rubbery membranes and in the stiff polystyrene membrane are large. The polymer chains in rubbers are considerably more flexible and rotate more easily than

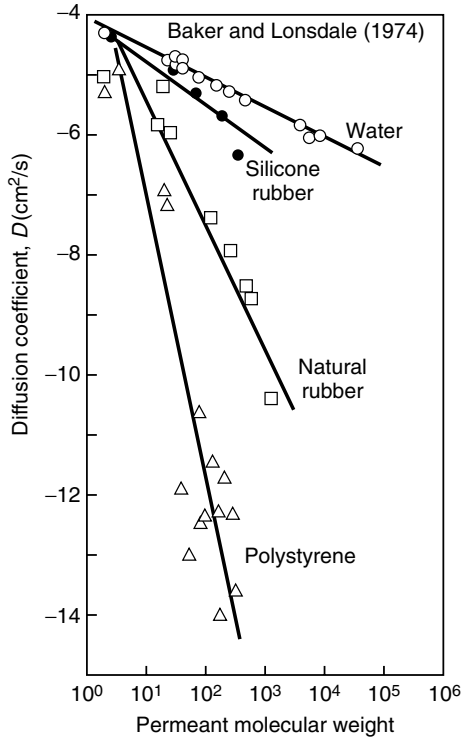

Figure 2.20 Permeant diffusion coefficient as a function of permeant molecular weight in water, natural rubber, silicone rubber and polystyrene. Diffusion coefficients of solutes in polymers usually lie between the value in natural rubber, an extremely permeable polymer, and the value in polystyrene, an extremely impermeable material [28]

those in polystyrene. One manifestation of this difference in chain flexibility is the difference in elastic properties; another is the difference in diffusion coefficient.

An example of the change in diffusion coefficient as the matrix material changes is illustrated by Figure 2.21. In this example, the polymer matrix material is changed by plasticization of the polymer, ethyl cellulose, by the permeant, dichloroethane [29]. The resulting change in the diffusion coefficient is shown in the figure. The concentration of dichloroethane in the polymer matrix increases from very low levels ($<1\,\%$ dichloroethane) to very high levels ($>90\,\%$ dichloroethane). As the concentration of dichloroethane increases, the polymer changes from a glassy polymer to a rubbery polymer, to a solvent-swollen gel, and finally to a dilute polymer solution. Ethyl cellulose is a glassy polymer with a glass transition of about $45-50\,^{\circ}\mathrm{C}$. At low concentrations of dichloroethane (below about 5 vol %) in the polymer, the ethyl cellulose matrix is glassy, and the dichloroethane diffusion coefficient is in the range 1 to 5×10^{-9} cm^2/s. As

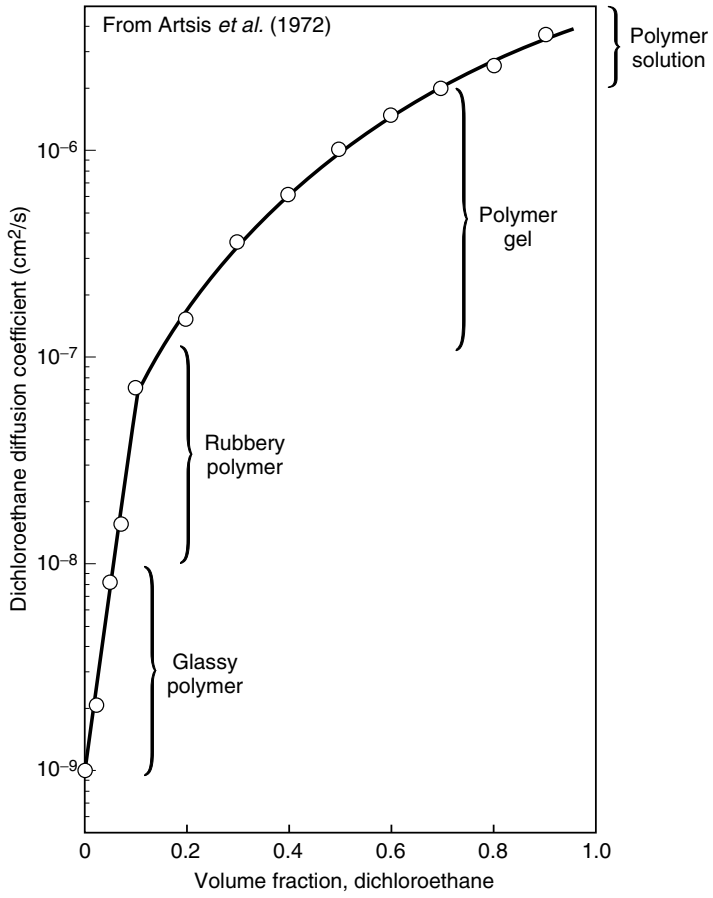

Figure 2.21 Changes in the diffusion coefficient of dichloroethane in ethyl cellulose as a function of the volume fraction of dichloroethane dissolved in the polymer matrix. Data of Artsis *et al*. [29]

the dichloroethane concentration increases to above 5 vol %, enough solvent has dissolved in the polymer to reduce the glass transition temperature to below the temperature of the experiment. The polymer chains then have sufficient freedom to rotate, and the polymer becomes rubbery. As the dichloroethane concentration increases further, the polymer chain mobility also increases as does the diffusion coefficient of dichloroethane. At 20 % dichloroethane, the diffusion coefficient is 1×10^{-7} cm^2/s, 100 times greater than the diffusion coefficient in the glassy polymer. Above 20 vol % dichloroethane, sufficient solvent is present to allow relatively large segments of the polymer chain to move. In this range, between 20 and 70 vol % dichloroethane, the matrix is best characterized as a solvent-swollen

gel, and the diffusion coefficient of dichloroethane increases from 1×10^{-7} to 2×10^{-6} cm^2/s. Finally, at dichloroethane concentrations above 70 vol %, sufficient solvent is present for the matrix to be characterized as a polymer solution. In this final solvent concentration range, the increase in diffusion coefficient with further increases in dichloroethane concentration is relatively small.

Figures 2.20 and 2.21 show the significant difference between diffusion in liquids and in rubbery and glassy polymers. A great deal of work has been performed over the last two decades to achieve a quantitative link between the structure of polymers and their permeation properties. No such quantitative structure–property relationship is at hand or even in sight. What has been achieved is a set of semiempirical rules that allow the permeation properties of related families of polymers to be correlated based on small changes in their chemical structures. The correlating tool most generally used is the polymer's *fractional free volume* v_f (cm^3/cm^3), usually defined as

$$v_f = \frac{v - v_o}{v} \tag{2.88}$$

where v is the specific volume of the polymer (cm^3/g), that is, the reciprocal of the polymer density, and v_o is the volume occupied by the molecules themselves (cm^3/g). The free volume of a polymer is the sum of the many small spaces between the polymer chains in these amorphous, noncrystalline materials.

The free volume of a polymer can be determined by measuring the polymer's specific volume, then calculating the occupied volume (v_o) of the groups that form the polymer. Tables of the molar volume of different chemical groups have been prepared by Bondi [30] and Van Krevelen [31]. By summing the molar volume of all the groups in the polymer repeat unit, the occupied molar volume of the polymer can be calculated. The occupied volume obtained in this way is about 1.3 times larger than the Van der Waals volume of the groups. The factor of 1.3 occurs because some unoccupied space is inevitably present even in crystals at 0 K. The fractional free volumes of a number of important membrane materials are given in Table 2.2.

The concept of polymer free volume is illustrated in Figure 2.22, which shows polymer specific volume (cm^3/g) as a function of temperature. At high temperatures the polymer is in the rubbery state. Because the polymer chains do not pack perfectly, some unoccupied space—free volume—exists between the polymer chains. This free volume is over and above the space normally present between molecules in a crystal lattice; free volume in a rubbery polymer results from its amorphous structure. Although this free volume is only a few percent of the total volume, it is sufficient to allow some rotation of segments of the polymer backbone at high temperatures. In this sense a rubbery polymer, although solid at the macroscopic level, has some of the characteristics of a liquid. As the temperature of the polymer decreases, the free volume also decreases. At the glass transition temperature, the free volume is reduced to a point at which the

Table 2.2 Calculated fractional free volume for representative membrane materials at ambient temperatures (Bondi method)

Polymer	Polymer type	Glass transition temperature, T_g (°C)	Fractional free volume (cm^3/cm^3)
Silicone rubber	Rubber	−129	0.16
Natural rubber	Rubber	−73	0.16
Polycarbonate	Glass	150	0.16
Poly(phenylene oxide)	Glass	167	0.20
Polysulfone	Glass	186	0.16
6FDA-ODA polyimide	Glass	300	0.16
Poly(4-methyl-2-pentyne) (PMP)	Glass	>250	0.28
Poly(1-trimethylsilyl-1-propyne) (PTMSP)	Glass	>250	0.34

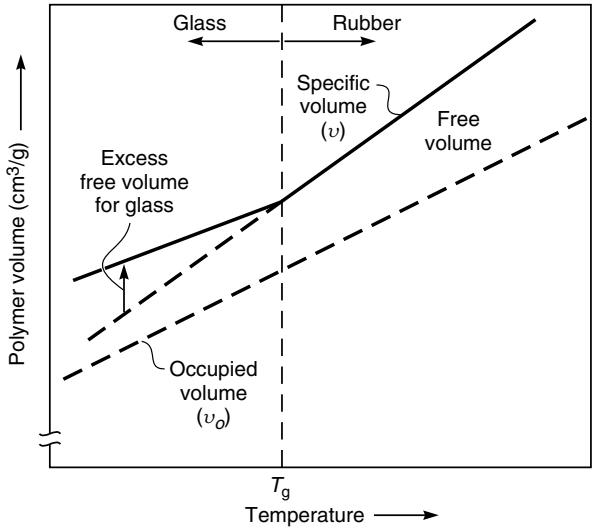

Figure 2.22 The change in specific volume as a function of temperature for a typical polymer

polymer chains can no longer rotate freely. Segmental motion then ceases, and the remaining free volume elements between the polymer chains are essentially frozen into the polymer matrix. As the polymer temperature is reduced further, its occupied volume will continue to decrease as the vibrational energy of the groups forming the polymer decreases, but the free volume elements remain essentially constant. Therefore, a glassy polymer contains both the normal free volume elements caused by the incomplete packing of the groups making up the polymer chains and the excess free volume elements frozen into the polymer matrix because the polymer chains cannot rotate.

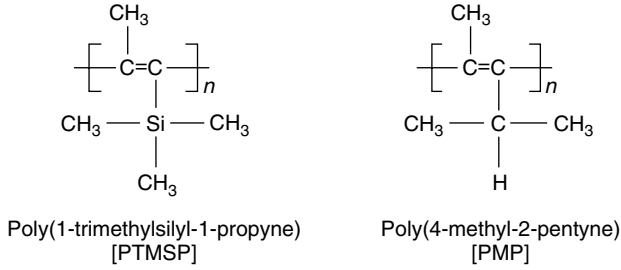

Figure 2.23 Structure of two high-free-volume substituted polyacetylenes, PTMSP and PMP. The carbon–carbon double bond is completely rigid, and depending on the size of the substituents, rotation around the carbon–carbon single bond can be very restricted also. The result is very stiff-backboned, rigid polymer chains which pack very poorly, leading to unusually high fractional free volumes

The fractional free volume of most materials is quite small and the value depends on the methods used for the calculation. For rubbers, the volume calculated by the Bondi method is generally about 10 to 15 % and for glassy polymers slightly higher, generally in the range 15 to 20 % because of the excess free volume contribution. Recently, a number of substituted polyacetylene polymers with extraordinarily rigid polymer backbones have been prepared. The structures of two such polymers are shown in Figure 2.23. Their glass transition temperatures are very high, and their free volumes are correspondingly unusually high—as much as 25 to 35 % of the polymers' volume is unoccupied space.

Correlation of the permeation properties of a wide variety of polymers with their free volume is not possible [32]. But, within a single class of materials, there is a correlation between the free volume of polymers and gas diffusion coefficients; an example is shown in Figure 2.24 [33]. The relationship between the free volume and the sorption and diffusion coefficients of gases in polymers, particularly glassy polymers, has been an area of a great deal of experimental and theoretical work. The subject has recently been reviewed in detail by Petropoulos [34] and by Paul and co-workers [35,36].

Sorption Coefficients in Polymers

The second key factor determining permeability in polymers is the sorption coefficient. The data in Figure 2.18 show that sorption coefficients for a particular gas are relatively constant within a single family of related materials. In fact, sorption coefficients of gases in polymers are relatively constant for a wide range of chemically different polymers. Figure 2.25 plots sorption and diffusion coefficients of methane in Tanaka's fluorinated polyimides [23], carboxylated polyvinyl trimethylsiloxane [37] and substituted polyacetylenes [38], all amorphous glassy polymers, and a variety of substituted siloxanes [39], all rubbers. The diffusion

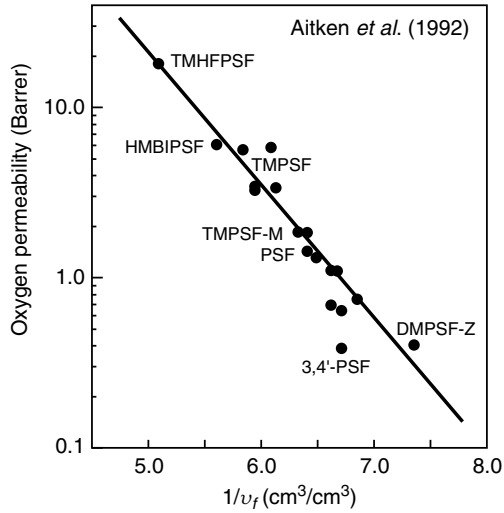

Figure 2.24 Correlation of the oxygen permeability coefficient for a family of related polysulfones with inverse fractional free volume (calculated using the Bondi method) [33]. Reprinted with permission from C.L. Aitken, W.J. Koros and D.R. Paul, Effect of Structural Symmetry on Gas Transport Properties of Polysulfones, *Macromolecules* **25**, 3424. Copyright 1992, American Chemical Society

coefficients of methane in the different polymers vary by more than 100 000, showing the extraordinary sensitivity of the permeant diffusion coefficients to changes in the packing of the polymer chains and to their flexibility. In contrast, sorption coefficients vary by only a factor of 10 around a mean value of about 15×10^{-3} cm^3(STP)/cm$^3 \cdot$ cmHg.

The sorption coefficients of gases in polymers remain relatively constant because sorption in polymers behaves as though the polymers were ideal fluids. Gas sorption in a polymer is expressed from Equation (2.57) as

$$c_{i_{(m)}} = K_i^{\mathrm{G}} p_i \tag{2.89}$$

By substituting for the sorption coefficient K_i^{G} from Equation (2.56), Equation (2.89) can be written as

$$c_{i_{(m)}} = m_i \rho_m \frac{\gamma_i^{\mathrm{G}} p_i}{\gamma_{i_{(m)}} p_{i_{\mathrm{sat}}}} \tag{2.90}$$

From the conversion of concentration to mole fraction [Equation (2.10)], it follows that

$$c_{i_{(m)}} = m_i \rho_m n_{i_{(m)}} \tag{2.91}$$

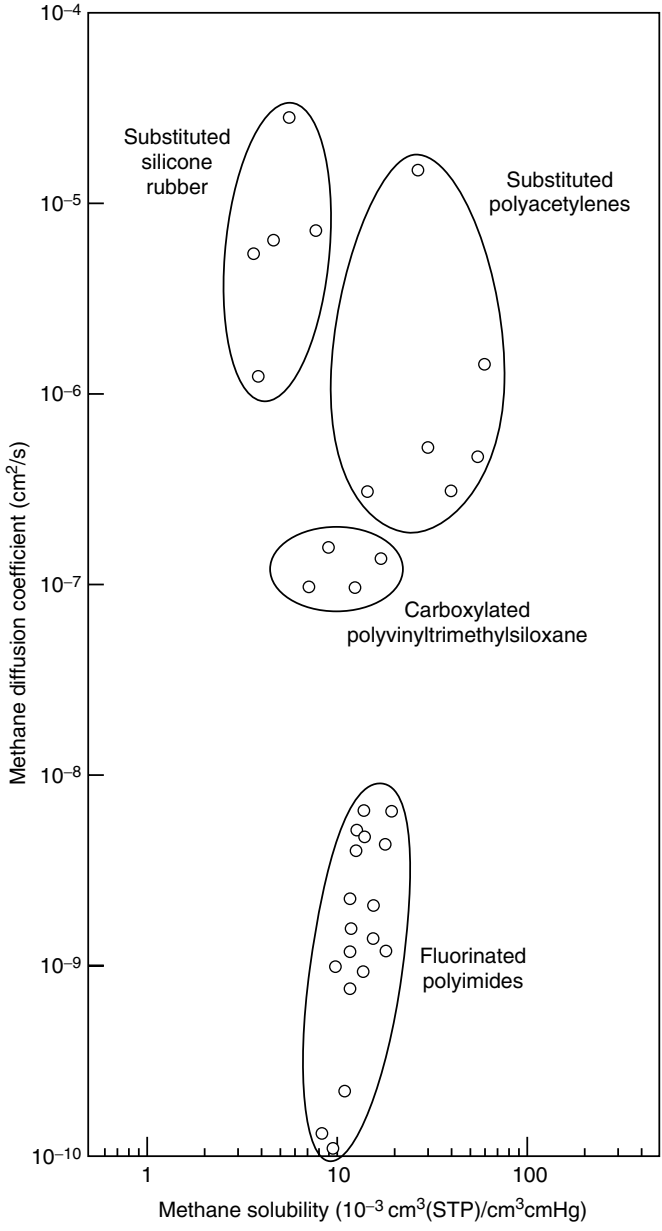

Figure 2.25 Diffusion and sorption coefficients of methane in different families of polymer materials. Diffusion coefficients change over a wide range but sorption coefficients are relatively constant. Data from references [23,35–37]

and so Equation (2.90) can be written as

$$\frac{c_{i_{(m)}}}{\rho_m m_i} = n_{i_{(m)}} = \frac{\gamma_i^{\mathrm{G}} p_i}{\gamma_{i_{(m)}} p_{i_{\mathrm{sat}}}} \tag{2.92}$$

For an ideal gas dissolving in an ideal liquid, γ_i^{G} and $\gamma_{i_{(m)}}$ are both unity, so Equation (2.92) can be written as

$$n_{i_{(m)}} = \frac{p_i}{p_{i_{\mathrm{sat}}}} \tag{2.93}$$

where $n_{i_{(m)}}$ is the mole fraction of the gas sorbed in the liquid, p_i is the partial pressure of the gas, and $p_{i_{\mathrm{sat}}}$ is the saturation vapor pressure at the pressure and temperature of the liquid. To apply Equation (2.93), the gas saturation vapor pressure must be determined. This can be done by extrapolating from available vapor pressure data to the ambient range using the Clausius–Clapeyron equation. For some gases the vapor pressure thereby obtained does not correspond to a stable gas–liquid equilibrium because the gas is supercritical at ambient temperatures. However, the calculated value is adequate to calculate the sorption coefficient using Equation (2.93) [40]. At 25 °C the saturation vapor pressure of methane extrapolated in this way is 289 atm. Thus, from Equation (2.93) the mole fraction of methane dissolved in an ideal liquid is 1/289 or 0.0035. The ideal solubility and measured solubilities of methane in a number of common liquids are given in Table 2.3. Although there is some spread in the data, particularly for small polar solvent molecules such as water or methanol, the overall agreement is remarkably good. A more detailed discussion of the solubility of gases in liquids is given in the book by Fogg and Gerrard [41].

To apply the procedure outlined above to a polymer, it is necessary to use the Flory–Huggins theory of polymer solution, which takes into account the entropy of mixing of solutes in polymers caused by the large difference in molecular size

Table 2.3 Mole fraction of methane in various solvents at 25 °C and 1 atm. The solubility of methane in an ideal liquid under these conditions is 0.0035 [40]

Liquid	Methane solubility (mole fraction)
Ethyl ether	0.0045
Cyclohexane	0.0028
Carbon tetrachloride	0.0029
Acetone	0.0022
Benzene	0.0021
Methanol	0.0007
Water	0.00002

between the two components. The Flory–Huggins expression for the free energy of mixing of a gas in polymer solution can be written [42]

$$\Delta G = RT \ln \frac{p_i}{p_{i_{\text{sat}}}} = RT \left[\ln V_i + \left(1 - \frac{\upsilon_i}{\upsilon_j}\right)(1 - V_i) \right] \tag{2.94}$$

where υ_i and υ_j are the molar volumes of the gas i and the polymer j respectively, and V_i the volume fraction of the polymer j occupied by the sorbed gas i. When $\upsilon_i \approx \upsilon_j$, that is, the gas and polymer molecules are approximately the same size, Equation (2.94) reduces to Equation (2.93), the ideal liquid case. When $\upsilon_i \ll \upsilon_j$, that is, when the molar volume of a gas (υ_i) is much smaller than the molar volume of the polymer (υ_j), then $\upsilon_i/\upsilon_j \to 0$ and Equation (2.94) becomes

$$\ln \frac{p_i}{p_{i_{\text{sat}}}} = \ln V_i + (1 - V_i) \tag{2.95}$$

Equation (2.95) can be rearranged to

$$V_i = \frac{p_i / p_{i_{\text{sat}}}}{\exp(1 - V_i)} \tag{2.96}$$

and since V_i is small, $\exp(1 - V_1)$ is approximately $\exp(1) \approx 2.72$, Equation (2.95) then becomes

$$V_i = \frac{p_i / p_{i_{\text{sat}}}}{2.72} \tag{2.97}$$

Comparing Equations (2.93) and (2.97), we see that the volume fraction of gas sorbed by an ideal polymer is 1/2.72 of the mole fraction of a gas sorbed in an ideal liquid.[6]

The results of such a calculation are shown in Table 2.4. In Figure 2.26, the calculated sorption coefficients in an ideal polymer from Table 2.4 are plotted against the average sorption coefficients of the same gases in Tanaka's polyimides [23]. The calculated values are within a factor of two of the experimental values, which is extremely good agreement considering the simplicity of Equation (2.97). A more detailed discussion of sorption of gases in polymers is given in a review by Petropoulos [34].

As shown above, thermodynamics can qualitatively predict the sorption of simple gases in polymers to within a factor of two. Moreover, Equation (2.97) predicts that all polymers should have about the same sorption for the same gas and that sorption is inversely proportional to saturation vapor pressure.

Another way of showing the same effect is to plot gas sorption against some convenient measure of saturation vapor pressure, such as the gas boiling point

[6] V_i is the volume fraction of the gas sorbed in the polymer. To calculate the amount of gas sorbed in cm^3 (STP)/cm^3, the molar density of the sorbed gas must be known. We assume this density is 1/MW (mol/cm^3).

Table 2.4 Solubility of gases in an ideal liquid and an ideal polymer (35 °C)

Gas	Calculated saturation vapor pressure, $p_{i_{sat}}$ (atm)	Ideal solubility in a liquid at 1 atm (mole fraction) [Equation (2.93)]	Ideal solubility in a polymer [10^{-3} $cm^3(STP)/cm^3 \cdot cmHg$] [Equation (2.97)]
N_2	1400	0.0007	2.6
O_2	700	0.0014	4.8
CH_4	366	0.0027	18.4
CO_2	79.5	0.0126	29.5

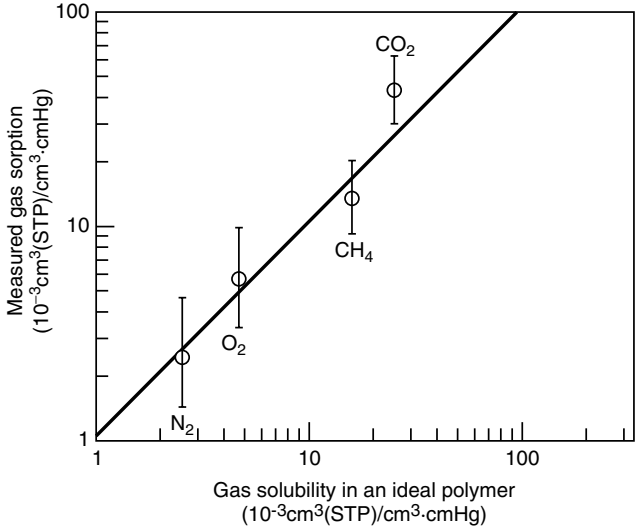

Figure 2.26 Average sorption coefficients of simple gases in a family of 18 related polyimides plotted against the expected sorption in an ideal polymer calculated using Equation (2.97). Data from Tanaka *et al.* [23]

or critical temperature. Figure 2.27 shows a plot of this type for a typical glassy polymer (polysulfone), a typical rubber (silicone rubber), and the values for the ideal solubility of a gas in a polymer calculated using Equation (2.97) [43]. The figure shows that the difference in gas sorptions of polymers is relatively small and the values are grouped around the calculated value.

Although all of these predictions are qualitatively correct, the differences between the behavior of an ideal polymer and an actual polymer are important in selecting the optimum material for a particular separation. The usual starting point for this fine-tuning is the dual-sorption model originally proposed by Barrer *et al.* [44]. This model has since been extended by Michaels *et al.* [45], Paul *et al.* [46], Koros *et al.* [47] and many others.

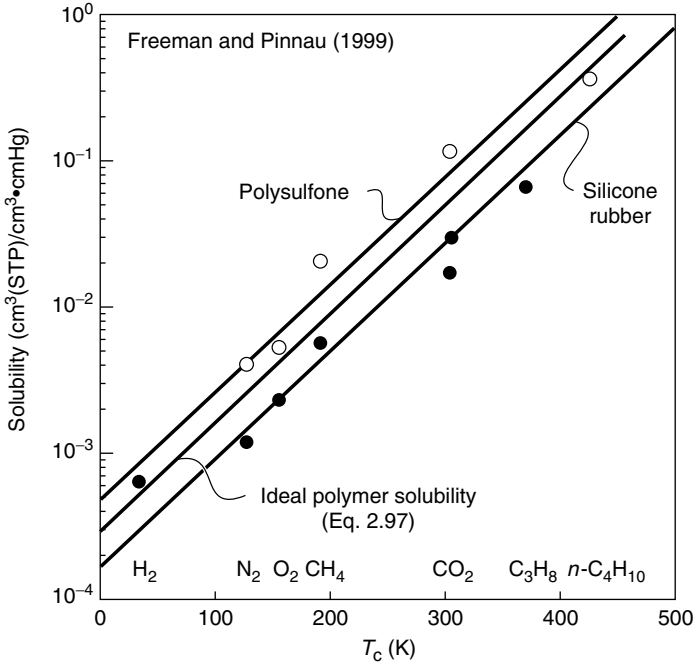

Figure 2.27 Solubilities as a function of critical temperature (T_c) for a typical glassy polymer (polysulfone) and a typical rubbery polymer (silicone rubber) compared with values for the ideal solubility calculated from Equation (2.97)[43]

According to the dual-sorption model, gas sorption in a polymer (c_m) occurs in two types of sites. The first type is filled by gas molecules dissolved in the equilibrium free volume portion of material (concentration c_H). In rubbery polymers this is the only population of dissolved gas molecules, but in glassy polymers a second type of site exists. This population of dissolved molecules (concentration c_D) is dissolved in the excess free volume of the glassy polymer. The total sorption in a glassy polymer is then

$$c_m = c_D + c_H \tag{2.98}$$

The number of molecules (c_D) dissolved in the equilibrium free volume portion of the polymer will behave as in normal sorption in a liquid and can be related to the pressure in the surrounding gas by a linear expression equivalent to Equation (2.89)

$$c_D = K_D p \tag{2.99}$$

This fraction of the total sorption is equivalent to the value calculated in Equation (2.97). The other fraction (c_H) is assumed to be sorbed into the excess

free volume elements, which are limited, so sorption will cease when all the sites are filled. Sorption in these sites is best approximated by a Langmuir-type absorption isotherm

$$c_H = \frac{c'_H bp}{1 + bp} \tag{2.100}$$

At high pressures $c_H \to c'_H$, where c'_H is the saturation sorption concentration at which all excess free volume sites are filled.

From Equations (2.99) and (2.100) it follows that the total sorption can be written as

$$c_m = K_D p + \frac{c'_H bp}{1 + bp} \tag{2.101}$$

The form of the sorption isotherm predicted from the dual sorption model is shown in Figure 2.28. Because the expressions for sorption contain three adjustable parameters, good agreement between theory and experiment is obtained.

Often, much is made of the particular values of the constants c'_H, b, and K. However, these constants should be treated with caution because they depend totally on the starting point of the curve-fitting exercise. That is, starting with an arbitrary value of c'_H, the other constants b and K can usually be adjusted to obtain good agreement of Equation (2.101) with experiment. If the starting value for c'_H is changed, then equally good agreement between theory and experiment can still be obtained but with different values of b and K [48].

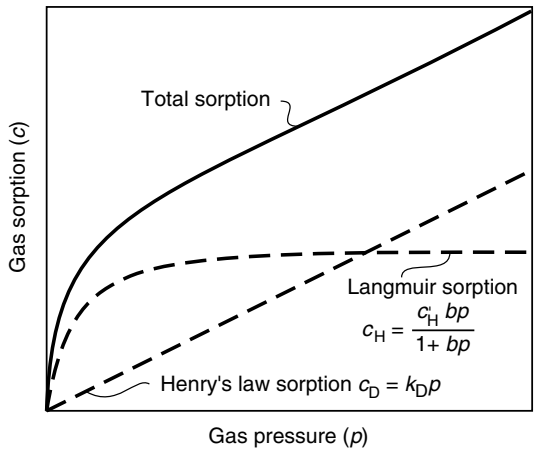

Figure 2.28 An illustration of the two components that contribute to gas sorption in a glassy polymer according to the dual sorption model. Henry's law sorption occurs in the equilibrium free volume portion of the polymer. Langmuir sorption occurs in the excess free volume between polymer chains that exists in glassy polymers

Permeation of gases in glassy polymers can also be described in terms of the dual sorption model. One diffusion coefficient (D_D) is used for the portion of the gas dissolved in the polymer according to the Henry's law expression and a second, somewhat larger, diffusion coefficient (D_H) for the portion of the gas contained in the excess free volume. The Fick's law expression for flux through the membrane has the form

$$J = -D_D \frac{dc_D}{dx} - D_H \frac{dc_H}{dx} \tag{2.102}$$

Pore-flow Membranes

The creation of a unified theory able to rationalize transport in the dense membranes used in reverse osmosis, pervaporation and gas separation occurred over a 20-year period from about 1960 to 1980. Development of this theory was one of the successes of membrane science. The theory did not form overnight as the result of one single breakthrough but rather as the result of a series of incremental steps. The paper of Lonsdale *et al.* [12] applying the solution-diffusion model to reverse osmosis for the first time was very important.[7] Also important was the series of papers by Paul and co-workers showing the connection between hydraulic permeation (reverse osmosis) and pervaporation [4–6, 19] and providing the experimental support for the solution-diffusion model as applied to these processes. Unfortunately no equivalent unified theory to describe transport in microporous membranes has been developed. Figure 2.29 illustrates part of the problem, namely the extremely heterogeneous nature of microporous membranes. All of the microporous membranes shown in this figure perform approximately the same separation, but their porous structure and the mechanism of the separation differ significantly. The nucleation track membrane (Figure 2.29a) and the asymmetric Loeb–Sourirajan membrane (Figure 2.29d) both separate particles by molecular sieving. The cellulose acetate/cellulose nitrate membrane (Figure 2.29c) is a depth filter which captures particles within the interior of the membrane by adsorption. The expanded film membrane (Figure 2.29b) captures particles by both methods. The materials from which these membranes are made also differ, ranging from polyethylene and polysulfone, both hydrophobic, low-surface-energy materials, to cellulose acetate, a hydrophilic material that often carries charged surface groups.

The parameters available to characterize the complexity of microporous membranes are also imperfect. Some widely used parameters are illustrated in Figure 2.30. The membrane porosity (ε) is the fraction of the total membrane

[7]This paper was initially submitted by its three industrial authors for publication to the *Journal of Physical Chemistry* and was rejected as insufficiently fundamental. More than 30 years after it was finally published in the *Journal of Applied Polymer Science*, it remains one of the most cited papers on membrane transport theory.

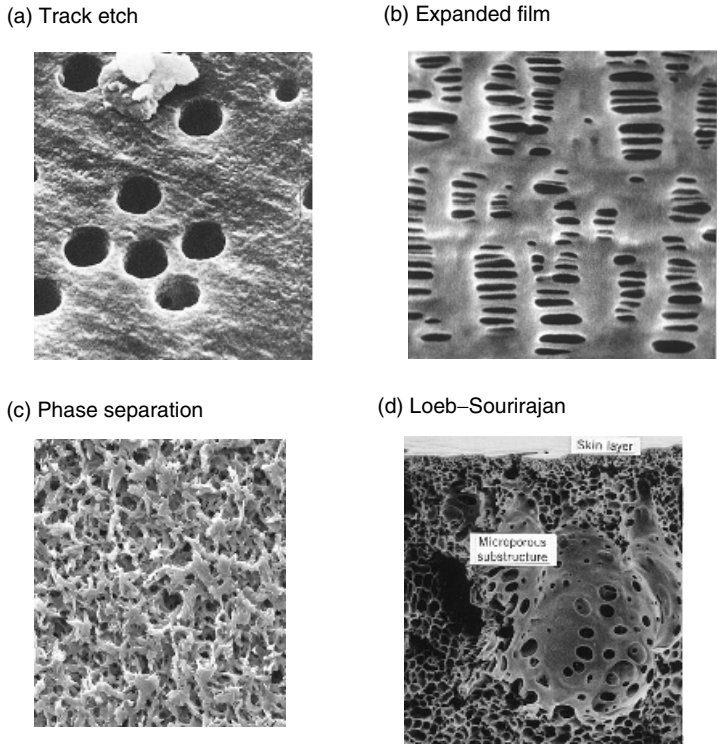

Figure 2.29 Scanning electron micrographs at approximately the same magnification of four microporous membranes having approximately the same particle retention. (a) Nuclepore (polycarbonate) nucleation track membrane; (b) Celgard® (polyethylene) expanded film membrane; (c) Millipore cellulose acetate/cellulose nitrate phase separation membrane made by water vapor imbibition (Courtesy of Millipore Corporation, Billerica, MA); (d) anisotropic polysulfone membrane made by the Loeb–Sourirajan phase separation process

volume that is porous. Typical microporous membranes have average porosities in the range 0.3–0.7. This number can be obtained easily by weighing the membrane before and after filling the pores with an inert liquid. The average porosity obtained this way must be treated with caution, however, because the porosity of a membrane can vary from place to place. For example, anisotropic membranes, such as the Loeb–Sourirajan phase separation membrane shown in Figure 2.29(d), often have an average porosity of 0.7–0.8, but the porosity of the skin layer that performs the actual separation may be as low as 0.05.

The membrane tortuosity (τ) reflects the length of the average pore compared to the membrane thickness. Simple cylindrical pores at right angles to the membrane surface have a tortuosity of one, that is, the average length of the pore is the

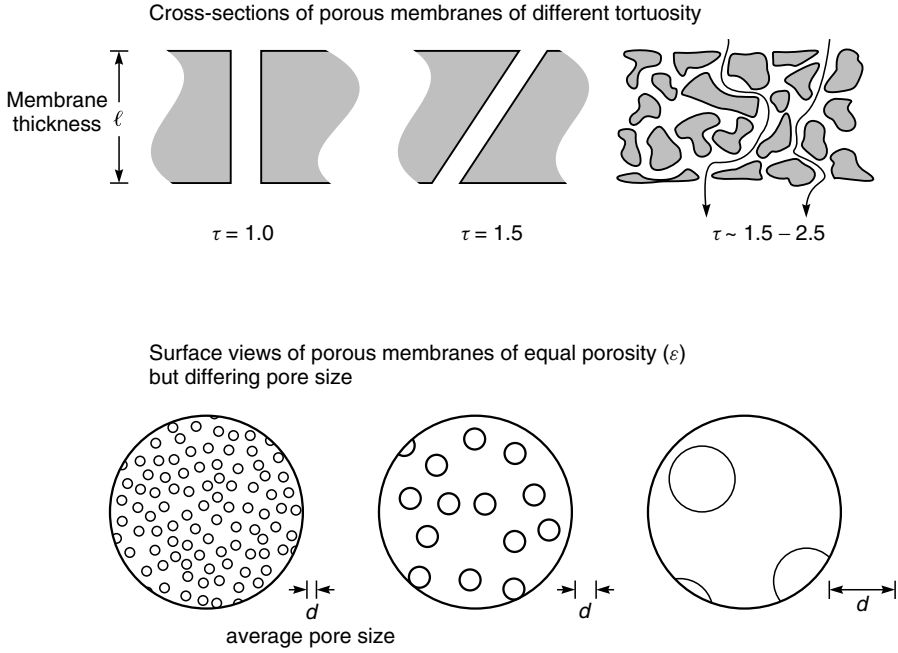

Figure 2.30 Microporous membranes are characterized by their tortuosity (τ), their porosity (ε), and their average pore diameter (d)

membrane thickness. Usually pores take a more meandering path through the membrane, so typical tortuosities are in the range 1.5–2.5.

The most important property characterizing a microporous membrane is the pore diameter (d). Some of the methods of measuring pore diameters are described in Chapter 7. Although microporous membranes are usually characterized by a single pore diameter value, most membranes actually contain a range of pore sizes. In ultrafiltration, the pore diameter quoted is usually an average value, but to confuse the issue, the pore diameter in microfiltration is usually defined in terms of the largest particle able to penetrate the membrane. This nominal pore diameter can be 5 to 10 times smaller than the apparent pore diameter based on direct microscopic examination of the membrane.

Permeation in Ultrafiltration and Microfiltration Membranes

Microporous ultrafiltration and microfiltration membranes used to filter particulates from liquids fall into the two general categories illustrated in Figure 2.31. The first category (a) is the surface or screen filter; such membranes contain surface pores smaller than the particles to be removed. Particles in the permeating

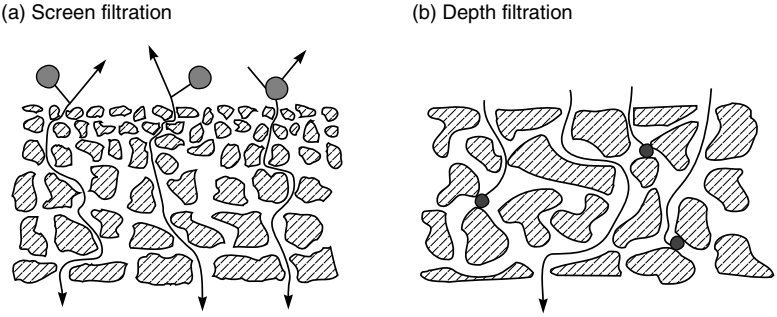

Figure 2.31 Separation of particulates can take place at the membrane surface according to a screen filtration mechanism (a) or in the interior of the membrane by a capture mechanism as in depth filtration (b)

fluid are captured and accumulate on the surface of the membrane. These membranes are usually anisotropic, with a relatively finely microporous surface layer on a more open microporous support. Particles small enough to pass through the surface pores are not normally captured in the interior of the membrane. Most ultrafiltration membranes are screen filters.

The second category of microporous membranes is the depth filter (b), which captures the particles to be removed in the interior of the membrane. The average pore diameter of a depth filter is often 10 times the diameter of the smallest particle able to permeate the membrane. Some particles are captured at small constrictions within the membrane, others by adsorption as they permeate the membrane by a tortuous path. Depth filters are usually isotropic, with a similar pore structure throughout the membrane. Most microfiltration membranes are depth filters.

Screen Filters

The mechanism of particle filtration by screen filters has been the subject of many studies because it is relatively easily described mathematically; Bungay has published a review of this work [49]. Ferry [50] was the first to model membrane retention by a screen filter; in his model pores were assumed to be equal circular capillaries with a large radius, r, compared to the solvent molecule radius. Therefore, the total area of the pore is available for transport of solvent. A solute molecule whose radius, a, is an appreciable fraction of the pore radius cannot approach nearer than one molecular radius of the pore overall. The model is illustrated in Figure 2.32.

The area, A, of the pore available for solute transport is given by the equation

$$\frac{A}{A_o} = \frac{(r-a)^2}{r^2} \tag{2.103}$$

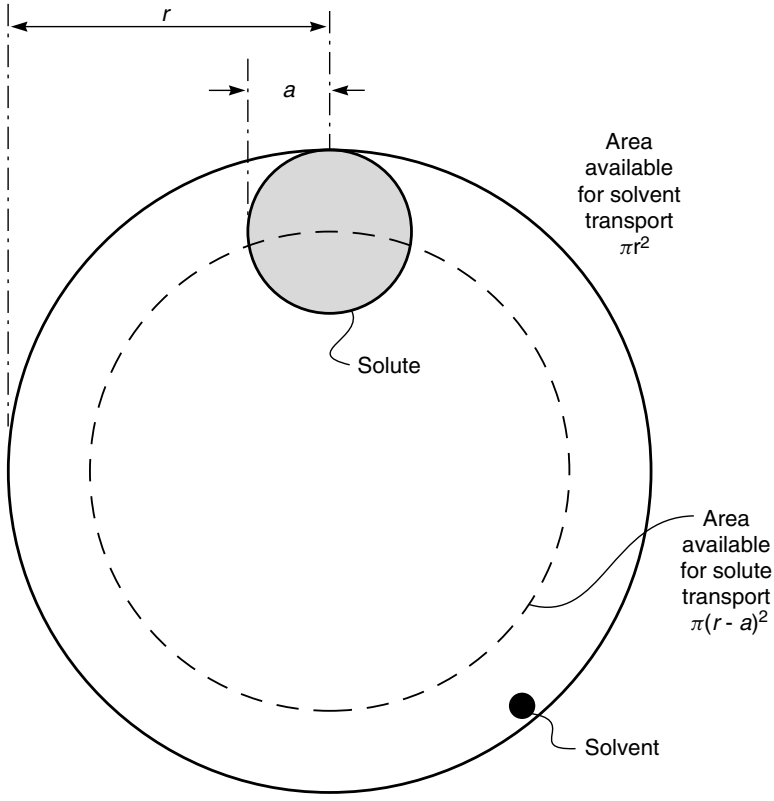

Figure 2.32 Illustration of the Ferry mechanical exclusion model of solute transport in small pores

where A_o is the area of the pore available for solvent molecules. Later, Renkin [51] showed that Equation (2.103) has to be modified to account for the parabolic velocity profile of the fluid as it passes through the pore. The effective fractional pore area available for solutes in this case is

$$\left(\frac{A}{A_o}\right)' = 2\left(1 - \frac{a}{r}\right)^2 - \left(1 - \frac{a}{r}\right)^4 \tag{2.104}$$

where $(A/A_o)'$ is equal to the ratio of the solute concentration in the filtrate (c_ℓ) to the concentration in the feed (c_o), that is,

$$\left(\frac{A}{A_o}\right)' = \left(\frac{c_\ell}{c_o}\right) \tag{2.105}$$

It follows that from Equation (2.105) and the definition of solution rejection [Equation (2.48)] that the rejection of the membrane is

$$\mathbb{R} = \left[1 - 2\left(1 - \frac{a}{r}\right)^2 + \left(1 - \frac{a}{r}\right)^4\right] \times 100\,\% \tag{2.106}$$

The Ferry–Renkin equation can be used to estimate the pore size of ultrafiltration membranes from the membrane's rejection of a solute of known radius. The rejections of globular proteins by four typical ultrafiltration membranes plotted against the cube root of the protein molecular weight (an approximate measure of the molecular radius) are shown in Figure 2.33(a). The theoretical curves

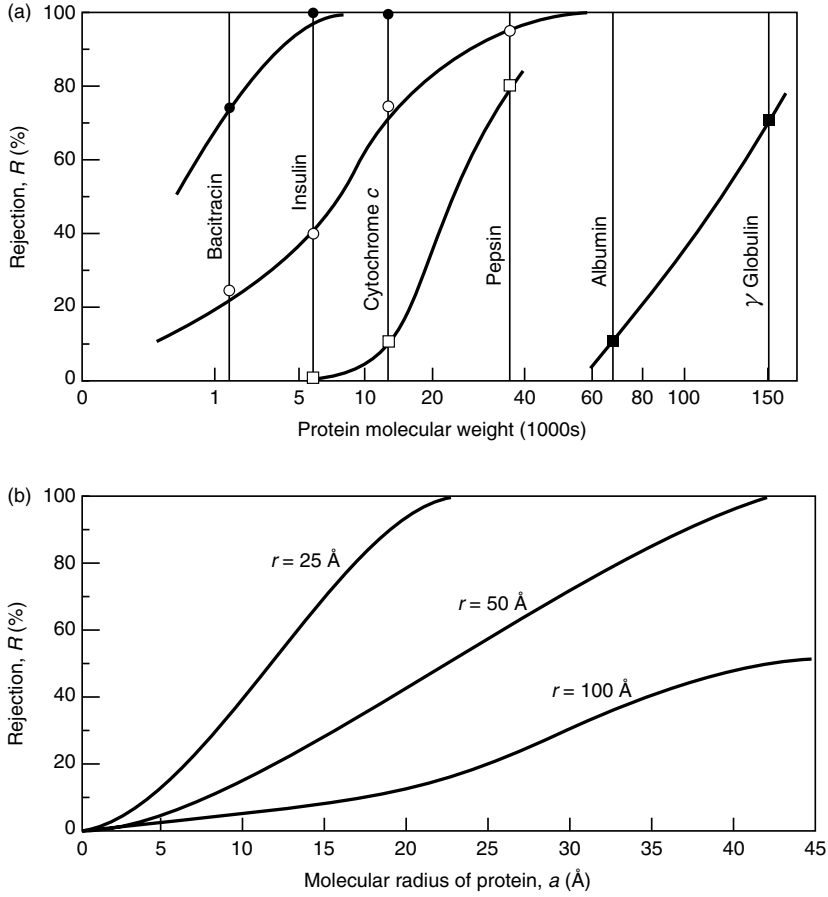

Figure 2.33 (a) Rejection of globular proteins by ultrafiltration membranes of increasing pore size; (b) calculated rejection curves from the Ferry–Renkin equation (2.106) plotted on the same scale [52]

Table 2.5 Marker molecules used to characterize ultrafiltration membranes

Species	Molecular weight ($\times 1000$)	Estimated molecular diameter (Å)
Sucrose	0.34	11
Raffinose	0.59	13
Vitamin B_{12}	1.36	17
Bacitracin	1.41	17
Insulin	5.7	27
Cytochrome *c*	13.4	38
Myoglobin	17	40
α-Chymotrysinogene	25	46
Pepsin	35	50
Ovalbumin	43	56
Bovine albumin	67	64
Aldolase	142	82
γ-Globulin	150	84

calculated from Equation (2.106) are shown directly in Figure 2.33(b) [52]. The abscissae of both figures have been made comparable because the radius of gyration of albumin is approximately 30 Å. A pore size that appears to be reasonable can then be obtained by comparing the two graphs. This procedure for obtaining an approximate pore size from membrane retention measurements shown in Figure 2.33 has been widely used. Globular proteins are usually the basis for this work because their molecular weights and molecular diameter can be calculated precisely. A list of some commonly used molecular markers is given in Table 2.5.

Depth Filters

The mechanism of particle capture by depth filtration is more complex than for screen filtration. Simple capture of particles by sieving at pore constructions in the interior of the membrane occurs, but adsorption of particles on the interior surface of the membrane is usually at least as important. Figure 2.34 shows four mechanisms that contribute to particle capture in depth membrane filters. The most obvious mechanism, simple sieving and capture of particles at constrictions in the membrane, is often a minor contributor to the total separation. The three other mechanisms, which capture particles by adsorption, are inertial capture, Brownian diffusion and electrostatic adsorption [53,54]. In all cases, particles smaller than the diameter of the pore are captured by adsorption onto the internal surface of the membrane.

In inertial capture, relatively large particles in the flowing liquid cannot follow the fluid flow lines through the membrane's tortuous pores. As a result, such particles are captured as they impact the pore wall. This capture mechanism is

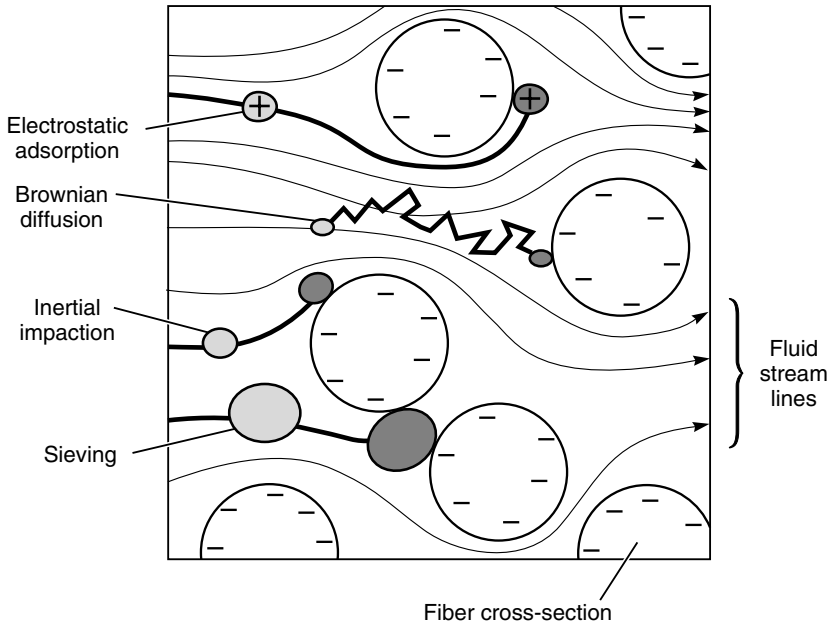

Figure 2.34 Particle capture mechanism in filtration of liquid solutions by depth microfilters. Four capture mechanisms are shown: simple sieving; electrostatic adsorption; inertial impaction; and Brownian diffusion

more frequent for larger diameter particles. In experiments with colloidal gold particles and depth filtration membranes with tortuous pores approximately 5 μm in diameter, Davis showed that 60 % of 0.05-μm-diameter particles were captured [55]. Nucleation track membranes with 5-μm, almost straight-through pores and no tortuosity retained less than 1 % of the particles. The retention of the small particles by the depth filter was caused by the greater tortuosity which led to inertial capture.

The second mechanism is capture by Brownian diffusion, which is more of a factor for smaller particles. Small particles are easily carried along by the moving fluid. However, because the particles are small, they are subject to random Brownian motion that periodically brings them into contact with the pore walls. When this happens, capture by surface adsorption occurs.

The third mechanism is capture of charged particles by membranes having surface-charged groups. Many common colloidal materials carry a slight negative charge, so membranes containing an excess of positive groups can provide enhanced removals. Several microfiltration membrane manufacturers produce this type of charged membrane. One problem is that the adsorption capacity of the charged group is exhausted as filtration proceeds, and the retention falls.

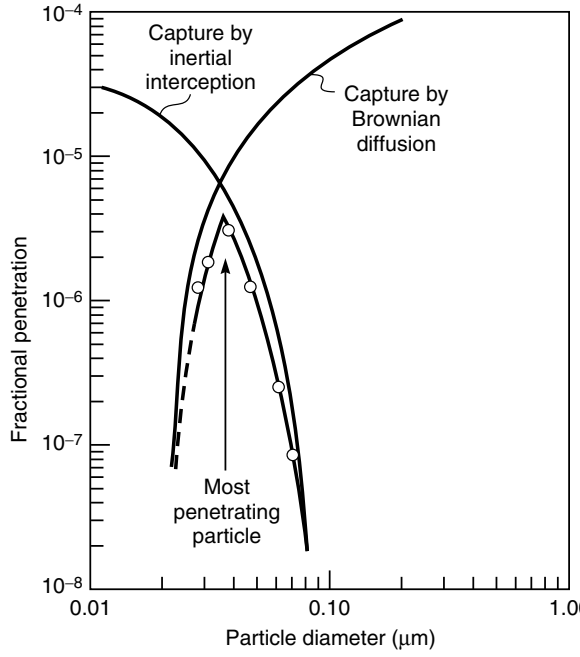

Figure 2.35 Gas-borne particle penetration through an ultrathin PVDF membrane [55,56]

In filtration of gas-borne aerosol particles by microfiltration membranes, capture by adsorption is usually far more important than capture by sieving. This leads to the paradoxical result that the most penetrating particle may not be the smallest one. This is because capture by inertial interception is most efficient for larger particles, whereas capture by Brownian motion is most efficient for smaller particles. As a result the most penetrating particle has an intermediate diameter, as shown in Figure 2.35 [55,56].

Knudsen Diffusion and Surface Diffusion in Microporous Membranes

Essentially all industrial gas separation membranes involve permeation through dense polymeric membranes. But the study of gas permeation through finely microporous membranes has a long history dating back to Graham's work in the 1850s. To date, the only application of these membranes has been the separation of $U^{235}F_6$ and $U^{238}F_6$ in the Manhattan project. More recently finely microporous membranes made by carbonizing poly(vinylidene chloride) and other polymers have been developed and taken to the pilot plant scale.

If the pores of a microporous membrane are 0.1 μm or larger, gas permeation will take place by normal convective flow described by Poiseuille's law. As

the pore radius (r) decreases it can become smaller than the mean free path (λ) of the gas. (At atmospheric pressure the mean free path of common gases is in the range 500–2000 Å.) When this occurs the ratio of the pore radius to the gas mean free path (r/λ) is less than one. Diffusing gas molecules then have more collisions with the pore walls than with other gas molecules. Gas permeation in this region is called Knudsen diffusion. At every collision with the pore walls, the gas molecules are momentarily adsorbed and then reflected in a random direction. Molecule–molecule collisions are rare, so each gas molecule moves independently of all others. Hence with gas mixtures in which the different species move at different average velocities, a separation is possible. The gas flow in a membrane made of cylindrical right capillaries for Knudsen diffusion is given by Equation (2.103)

$$j = \frac{4r\varepsilon}{3} \cdot \left(\frac{2RT}{\pi m}\right)^{1/2} \cdot \frac{p_o - p_\ell}{\ell \cdot RT} \tag{2.107}$$

where m is the molecular weight of the gas, j is the flux in gmol/cm$^2 \cdot$ s, ε is the porosity of the membrane, r is the pore radius, ℓ is the pore length and p_o and p_ℓ are the absolute pressures of the gas species at the beginning of the pore ($x = 0$) and at the end ($x = \ell$).

The equivalent equation for permeation by Poiseuille flow is

$$j = \frac{r^2\varepsilon}{8\eta} \cdot \frac{[p_o - p_\ell][p_o + p_\ell]}{\ell \cdot RT} \tag{2.108}$$

where η is the viscosity of the gas. Equation (2.108) differs from the more familiar Poiseuille equation for liquids by the additional term $[p_o + p_\ell]$ which arises from the expansion of a gas as it moves down the pressure gradient.

Figure 2.36 shows the effect of the ratio r/λ on the relative proportions of Knudsen to Poiseuille flow in a cylindrical capillary [57]. When r/λ is greater than one, Poiseuille flow predominates. Because the mean free path of gases at atmospheric pressure is in the range of 500–2000 Å, for Knudsen flow to predominate and a separation to be obtained, the membrane pore radius must be less than 500 Å.

It follows from Equation (2.107) that the permeability of a gas (i) through a Knudsen diffusion membrane is proportional to $1/\sqrt{m_i}$. The selectivity of this membrane ($\alpha_{i/j}$), proportional to the ratio of gas permeabilities, is given by the expression

$$\alpha_{i/j} = \sqrt{\frac{m_j}{m_i}} \tag{2.109}$$

This result was first observed experimentally by Graham and is called Graham's law of diffusion. Knudsen diffusion membranes have been used to separate gas isotopes that are difficult to separate by other methods, for example tritium from

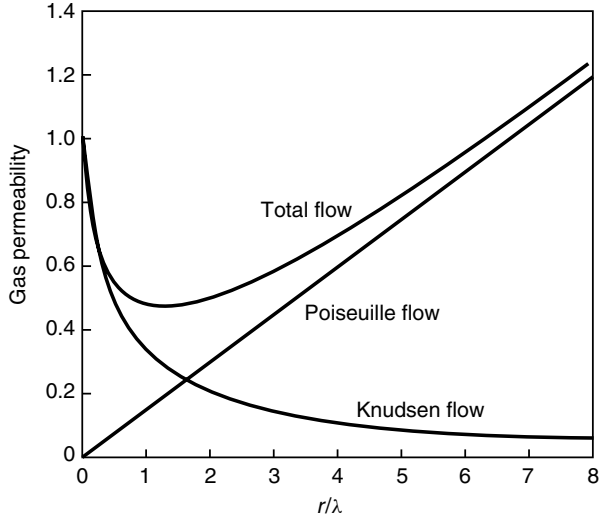

Figure 2.36 Illustration of the proportion of Knudsen to Poiseuille flow as a function of r/λ (after Barrer) [57]

hydrogen, $C^{12}H_4$ from $C^{14}H_4$ and most importantly $U^{235}F_6$ from $U^{238}F_6$. The membrane selectivity for $U^{235}F_6/U^{238}F_6$ mixtures is only 1.0043, so hundreds of separation stages are required to produce a complete separation. Nevertheless, at the height of the Cold War, the US Atomic Energy Commission operated three plants fitted with microporous metal membranes that processed almost 20 000 tons/year of uranium.

When the pore diameter of a microporous membrane decreases to the 5–10 Å range, the pores begin to separate gases by a molecular sieving effect. The difficulty of making these membranes defect-free has so far prevented their application to industrial separations. However, in the laboratory, spectacular separations have been reported for gases that differ in size by only 0.1 Å. Figure 2.37 shows some data for permeation through microporous silica membranes [58]. No polymeric membranes can match this separation.

Surface adsorption and diffusion add a second contribution to gas permeation that can occur in small-pore-diameter membranes. This phenomenon is shown schematically in Figure 2.38. Adsorption onto the walls of the small pores becomes noticeable when the pore diameter drops below about 100 Å. At this pore diameter the surface area of the pore walls is in the range 100 m^2/cm^3 of material. Significant amounts of gas then adsorb onto the pore walls, particularly if the gas is condensable. Often the amount of gas sorbed on the pore walls is much greater than the amount of nonsorbed gas. Sorbed gas molecules are mobile and can move by a process of surface diffusion through the membrane according

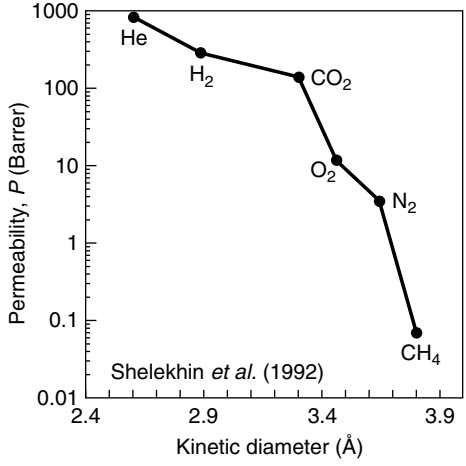

Figure 2.37 Permeability coefficients as a function of the gas kinetic diameter in microporous silica hollow fine fibers [58]. Reprinted from *J. Membr. Sci.* **75**, A.B. Shelekhin, A.G. Dixon and Y.H. Ma, Adsorption, Permeation, and Diffusion of Gases in Microporous Membranes, 233, Copyright 1992, with permission from Elsevier

to a Fick's law type of expression

$$J_s = -D_s \frac{\mathrm{d}c_s}{\mathrm{d}x} \tag{2.110}$$

where J_s is the contribution to permeation by surface diffusion of the sorbed gas c_s and D_s is a surface diffusion coefficient. At room temperature, typical surface diffusion coefficients are in the range 1×10^{-3}–1×10^{-4} cm^2/s, intermediate between the diffusion coefficients of molecules in gases and liquids [59]. Although these coefficients are less than the diffusion coefficients for nonsorbed gas, surface diffusion still makes a significant contribution to total permeation.

Some typical results illustrating the effect of surface diffusion are shown in Figure 2.39 for permeation of gases through microporous glass [60]. The expected permeability normalized for gas molecular weight, $\mathcal{P}\sqrt{m}$, is constant, but only the very low boiling gases, helium, hydrogen and neon, approach this value. As the condensability of the gas increases (as measured by boiling point or critical temperature) the amount of surface adsorption increases and the contribution of surface diffusion to gas permeation increases. For butane, for example, 80 % of the total gas permeation is due to surface diffusion.

In experiments with mixtures of condensable and noncondensable gases, adsorption of the condensable gas component can restrict or even completely block permeation of the noncondensable gas [61,62]. This effect was first noticed by Barrer and Pope in experiments with sulfur dioxide/hydrogen mixtures [63]; some of the data are shown in Figure 2.40. Sorption of sulfur dioxide on the pore walls

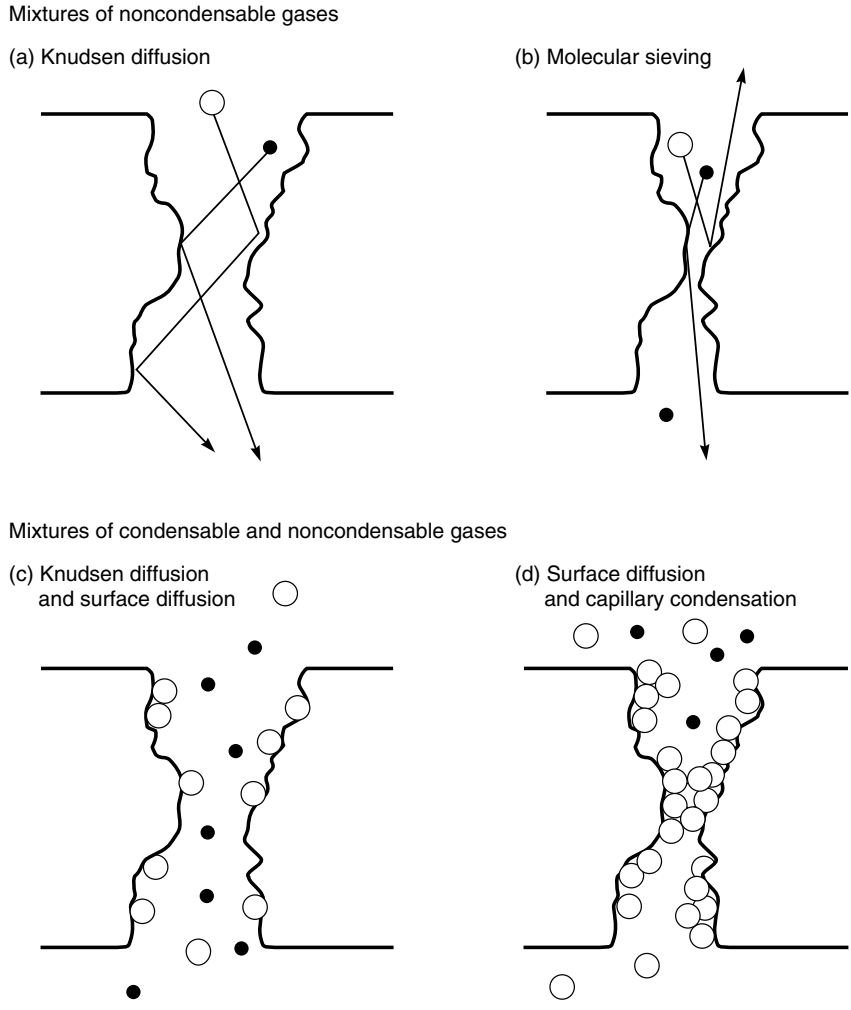

Figure 2.38 Permeation of noncondensable and condensable gas mixtures through finely microporous membranes. With noncondensable gases molecular sieving occurs when the pore wall reaches the 5- to 10-Å diameter range. With gas mixtures containing condensable gases surface diffusion increases as the pore diameter decreases and the temperature decreases (increasing adsorption)

of the microporous carbon membrane inhibits the flow of hydrogen. If adsorption is increased by increasing the sulfur dioxide partial pressure or by lowering the temperature, sufficient sulfur dioxide is adsorbed to cause capillary condensation of sulfur dioxide in the membrane pores, completely blocking permeation of hydrogen. At this point the membrane only permeates sulfur dioxide.

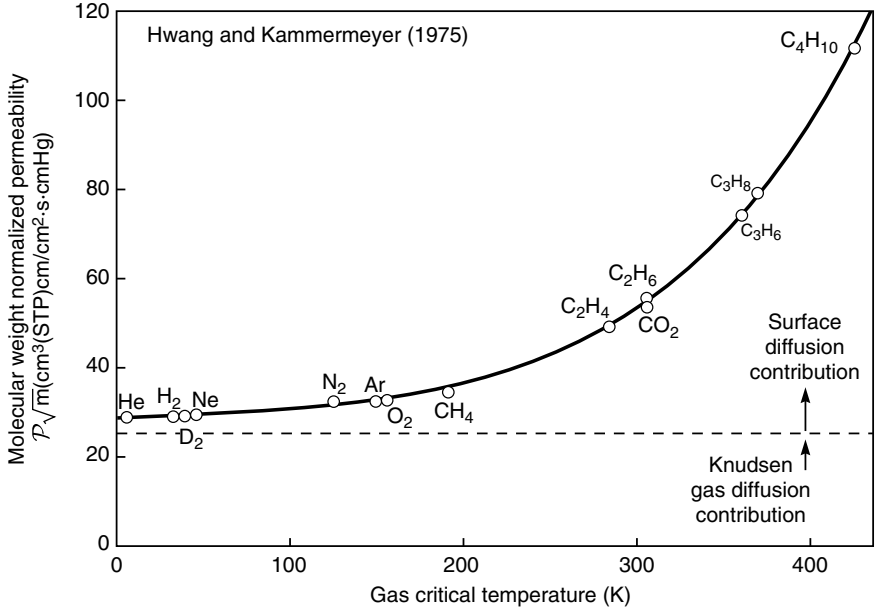

Figure 2.39 Molecular-weight-normalized permeability of gases through Vycor microporous glass membranes [60]. Reprinted from *Techniques of Chemistry, Vol. VII, Membranes in Separations*, S.T. Hwang and K. Kammermeyer; A. Weissberger (ed.); Copyright © 1975. This material is used by permission of John Wiley & Sons, Inc.

Microporous carbonized hollow fibers were developed over a period of 20 years by Soffer, Koresh, and others (64) at Carbon Membranes Ltd. and were brought to the small module scale. Spectacular separations were reported, but the membranes were difficult to make defect-free and were relatively sensitive to fouling and breaking. More recently, Rao, Sirkar, and others at Air Products tried to use microporous membranes to separate hydrogen/light hydrocarbon gas mixtures found in refinery waste gas streams [65,66]. They also used microporous carbon membranes, this time formed by vacuum carbonization of polymer films cast onto microporous ceramic supports. The adsorbed hydrocarbons permeate the membranes by surface diffusion while permeation of hydrogen in the gas phase is blocked by capillary condensation in the membrane pores. The process was tried at the pilot-plant scale, but eventually abandoned in part because of blocking of the membranes by permanently adsorbed higher hydrocarbons in the feed gas.

Despite these failures, microporous carbon membranes continue to be a subject of research by a number of groups [67–70]. The selectivities obtained are often very good, even for simple gas mixtures such as oxygen/nitrogen or carbon dioxide/methane. However long-term, it is difficult to imagine carbon membranes

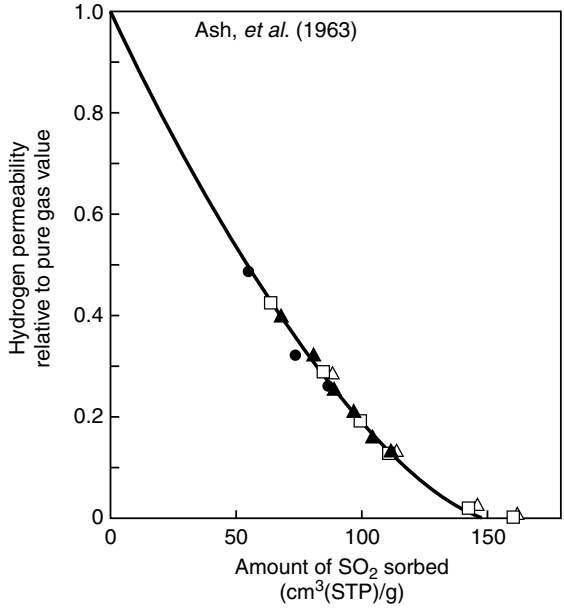

Figure 2.40 Blocking of hydrogen in hydrogen/sulfur dioxide gas mixture permeation experiments with finely microporous membranes [63] as a function of the amount of sulfur dioxide adsorbed by the membrane. As sulfur dioxide sorption increases the hydrogen permeability is reduced until at about 140 $cm^3(SO_2)(STP)/g$, the membrane is completely blocked and only sulfur dioxide permeates. Data obtained at several temperatures fall on the same master curve (●, 0 °C; ▲, −10 °C; □, −20.7 °C; △, −33.6 °C). Reprinted from R. Ash, R.M. Barrer and C.G. Pope, Flow of Adsorbable Gases and Vapours in Microporous Medium, *Proc. R. Soc. London, Ser. A*, **271**, 19 (1963) with permission from The Royal Society

competing with polymeric membranes for these separations. Carbon membranes are likely to be 10 to 100 times more expensive than equivalent polymeric membranes. This cost differential can only be tolerated in applications in which polymeric membranes completely fail to make the separation. Such applications might be the high-temperature separation of hydrocarbon vapor/vapor mixtures; the chemical and physical stability of ceramic and carbon membranes is a real advantage in this type of separation.

Although the literature of gas separation with microporous membranes is dominated by inorganic materials, polymer membranes have also been tried with some success. The polymers used are substituted polyacetylenes, which can have an extraordinarily high free volume, on the order of 25 vol %. The free volume is so high that the free volume elements in these polymers are probably interconnected. Membranes made from these polymers appear to function as finely microporous materials with pores in the 5 to 15 Å diameter range [71,72]. The two most

widely studied polyacetylenes are poly(1-trimethylsilyl-1-propyne) (PTMSP) and poly(4-methyl-2-pentyne) (PMP), with the structures shown in Figure 2.23. Gas permeabilities in these materials are orders of magnitude higher than those of conventional, low-free-volume glassy polymers, and are even substantially higher than those of poly(dimethylsiloxane), for many years the most permeable polymer known. The extremely high free volume provides a sorption capacity as much as 10 times that of a conventional glassy polymer. More dramatically, diffusion coefficients are 10^3 to 10^6 times greater than those observed in conventional glassy polymers. This combination of extraordinarily high permeabilities, together with the very high free volume, hints at a pore-flow contribution. Nonetheless, the ratio of the diffusion coefficients of oxygen and nitrogen (D_{O_2}/D_{N_2}) is 1.4, a small value for a glassy polymer membrane but still more than would be expected for a simple Knudsen diffusion membrane.

These high-free-volume polymers also have unusual permeability characteristics with mixtures of condensable and noncondensable gases. For example, in the presence of as little as 1200 ppm of a condensable vapor such as the perfluorocarbon FC-77 (a perfluoro octane-perfluoro decane mixture), the nitrogen permeability of PTMSP is 20 times lower than the pure nitrogen permeability [71], as shown in Figure 2.41. When the condensable vapor is removed from the feed gas the nitrogen permeability rapidly returns to its original value. The best

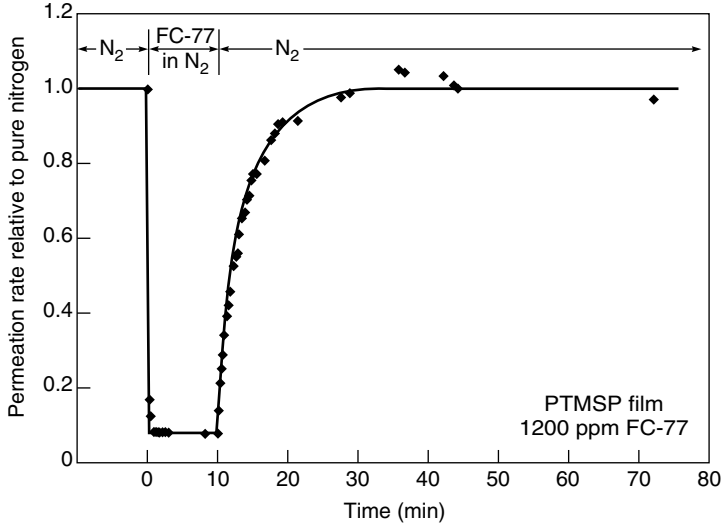

Figure 2.41 The change in nitrogen flux through a PTMSP membrane caused by the presence of a condensable vapor in the feed gas [71]. This behavior is characteristic of extremely finely porous microporous ceramic or ultrahigh-free-volume polymeric membranes such as PTMSP. The condensable vapor adsorbs in the 5- to 15-Å-diameter pores of the membrane, blocking the flow of the noncondensable nitrogen gas

explanation for these unusual vapor permeation properties is that PTMSP, because of its very high free volume, is an ultra-microporous membrane in which pore-flow transport occurs. The FC-77 vapor causes capillary condensation in which the pores are partially or completely blocked by the adsorbed vapor, preventing the flow of noncondensed gases (nitrogen) through the membrane.

The Transition Region

The transition between pore-flow and solution-diffusion transport seems to occur with membranes having very small pores. Ultrafiltration membranes that reject sucrose and raffinose but pass all micro-ions are clearly pore-flow membranes, whereas desalination-grade sodium-chloride-rejecting reverse osmosis membranes clearly follow the solution-diffusion model. Presumably, the transition is in the nanofiltration range, with membranes having good rejections to divalent ions and most organic solutes, but rejection of monovalent ions in the 20–70 % range. The performance of a family of nanofiltration membranes of this type is illustrated in Table 2.6 [73]. The FT30 membrane is clearly a good reverse osmosis membrane, whereas the XP-20 is a very small pore flow ultrafiltration membrane. The XP-45 membrane is intermediate in character.

The transition between reverse osmosis membranes with a salt rejection of more than 95 % and molecular weight cutoffs below 50 and ultrafiltration membranes with a salt rejection of less than 10 % and a molecular weight cutoff of more than 1000 is shown in Figure 2.42 [74]. The very large change in the pressure-normalized flux of water that occurs as the membranes become more retentive is noteworthy. Because these are anisotropic membranes, the thickness of the separating layer is difficult to measure, but clearly the permeability of

Table 2.6 Rejection of microsolutes by nanofiltration membranes (FilmTec data) [73]. Reprinted from *Desalination*, **70**, J. Cadotte, R. Forester, M. Kim, R. Petersen and T. Stocker, Nanofiltration Membranes Broaden the Use of Membrane Separation Technology, p. 77, Copyright 1988, with permission from Elsevier

Solute	Solute rejection (%)		
	FT-30	XP-45	XP-20
NaC1	99.5	50	20
$MgCl_2$	>99.5	83	—
$MgSO_4$	>99.5	97.5	85
$NaNO_3$	90	<20	0
Ethylene glycol	70	24	11
Glycerol	96	44	15
Glucose	99	95	60
Sucrose	100	100	89

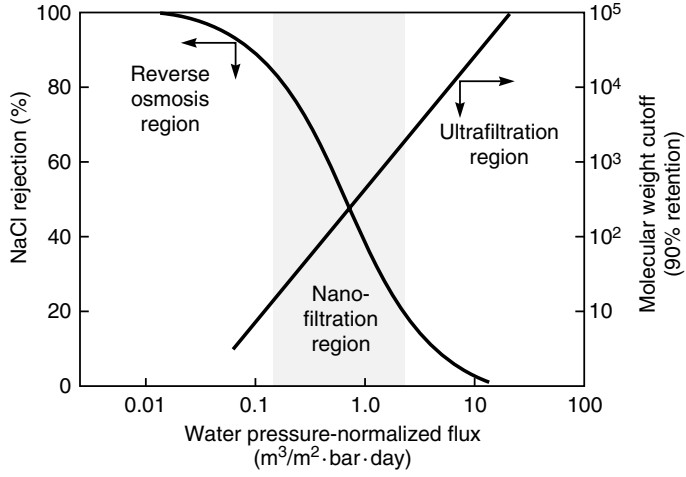

Figure 2.42 Diagram of the region of nanofiltration membrane performance relative to reverse osmosis and ultrafiltration membranes [74]

water through the pores of ultrafiltration membranes is orders of magnitude higher than permeability through dense solution-diffusion reverse osmosis membranes. Gas permeation also places high-free-volume substituted polyacetylene polymer membranes in the transition area between solution-diffusion and pore flow.

Conclusions and Future Directions

During the last 30 years the basis of permeation through membranes has become much clearer. This is particularly true for reverse osmosis, gas permeation and pervaporation for which the solution-diffusion model is now almost universally accepted and well-supported by a body of experimental evidence. This model provides simple equations that accurately link the driving forces of concentration and pressure with flux and selectivity. The solution-diffusion model has been less successful at providing a link between the nature of the membrane material and the membrane permeation properties. This link requires an ability to calculate membrane diffusion and sorption coefficients. These calculations require knowledge of the molecular level of interactions of permeant molecules and their motion in the polymer matrix that is not yet available. Only semiempirical correlations such as the dual sorption model or free volume correlations are available. The best hope for future progress towards *a priori* methods of calculating permeant sorption and diffusion coefficients lies in computer-aided molecular dynamic simulations, but accurate predictions using this technique are years—perhaps decades—away.

The theory of permeation through microporous membranes in ultrafiltration and microfiltration is much less developed and it is difficult to see a clear path forward. Permeation through these membranes is affected by a variety of hard-to-compute effects and is also very much a function of membrane structure and composition. Measurements of permeation through ideal uniform-pore-diameter membranes made by the nucleation track method are in good agreement with theory. Unfortunately, industrially useful membranes have nonuniform tortuous pores and are often anisotropic as well. Current theories cannot predict the permeation properties of these membranes.

References

1. S. Sourirajan, *Reverse Osmosis*, Academic Press, New York (1970).
2. H. Yasuda and A. Peterlin, Diffusive and Bulk Flow Transport in Polymers, *J. Appl. Polym. Sci.* **17**, 433 (1973).
3. P. Meares, On the Mechanism of Desalination by Reversed Osmotic Flow Through Cellulose Acetate Membrane, *Eur. Polym. J.* **2**, 241 (1966).
4. D.R. Paul and O.M. Ebra-Lima, Pressure-induced Diffusion of Organic Liquids Through Highly Swollen Polymer Membranes, *J. Appl. Polym. Sci.* **14**, 2201 (1970).
5. D.R. Paul, Diffusive Transport in Swollen Polymer Membranes, in *Permeability of Plastic Films and Coatings*, H.B. Hopfenberg (ed.), Plenum Press, New York, pp. 35–48 (1974).
6. D.R. Paul, The Solution-diffusion Model for Swollen Membranes, *Sep. Purif. Meth.* **5**, 33 (1976).
7. A. Fick, Über Diffusion, *Poggendorff's Annal. Physik Chem.* **94**, 59 (1855).
8. E. Smit, M.H.V. Mulder, C.A. Smolders, H. Karrenbeld, J. van Eerden and D. Feil, Modeling of the Diffusion of Carbon Dioxide in Polyimide Matrices by Computer Simulation, *J. Membr. Sci.* **73**, 247 (1992).
9. S.G. Charati and S.A. Stern, Diffusion of Gases in Silicone Polymers: Molecular Dynamic Simulations, *Macromolecules* **31**, 5529 (1998).
10. J.G. Wijmans and R.W. Baker, The Solution-diffusion Model: A Review, *J. Membr. Sci.* **107**, 1 (1995).
11. F. Theeuwes, R.M. Gale and R.W. Baker, Transference: a Comprehensive Parameter Governing Permeation of Solutes Through Membranes, *J. Membr. Sci.* **1**, 3 (1976).
12. H.K. Lonsdale, U. Merten and R.L. Riley, Transport Properties of Cellulose Acetate Osmotic Membranes, *J. Appl. Polym. Sci.* **9**, 1341 (1965).
13. U. Merten, Transport Properties of Osmotic Membranes, in *Desalination by Reverse Osmosis*, U. Merten (ed.), MIT Press, Cambridge, MA, pp. 15–54 (1966).
14. N. Bhore, R.M. Gould, S.M. Jacob, P.O. Staffeld, D. McNally, P.H. Smiley and C.R. Wildemuth, New Membrane Process Debottlenecks Solvent Dewaxing Unit, *Oil Gas J.* **97**, 67 (1999).
15. R.W. Baker and J.G. Wijmans, Membrane Separation of Organic Vapors from Gas Streams, in *Polymeric Gas Separation Membranes*, D.R. Paul and Y.P. Yampol'skii (eds), CRC Press, Boca Raton, FL, pp. 353–398 (1994).
16. T. Kataoka, T. Tsuro, S.-I. Nakao and S. Kimura, Membrane Transport Properties of Pervaporation and Vapor Permeation in an Ethanol–Water System Using Polyacrylonitrile and Cellulose Acetate Membranes, *J. Chem. Eng. Jpn* **24**, 326 (1991).
17. J.G. Wijmans and R.W. Baker, A Simple Predictive Treatment of the Permeation Process in Pervaporation, *J. Membr. Sci.* **79**, 101 (1993).

18. F.W. Greenlaw, W.D. Prince, R.A. Shelden and E.V. Thompson, Dependence of Diffusive Permeation Rates by Upstream and Downstream Pressures, *J. Membr. Sci.* **2**, 141 (1977).
19. D.R. Paul and D.J. Paciotti, Driving Force for Hydraulic and Pervaporation Transport in Homogeneous Membranes, *J. Polym. Sci., Polym. Phys. Ed.* **13**, 1201 (1975).
20. S. Rosenbaum and O. Cotton, Steady-state Distribution of Water in Cellulose Acetate Membrane, *J. Polym. Sci.* **7**, 101 (1969).
21. S.N. Kim and K. Kammermeyer, Actual Concentration Profiles in Membrane Permeation, *Sep. Sci.* **5**, 679 (1970).
22. D.R. Paul, J.D. Paciotti and O.M. Ebra-Lima, Hydraulic Permeation of Liquids Through Swollen Polymeric Networks, *J. Appl. Polym. Sci.* **19**, 1837 (1975).
23. K. Tanaka, H. Kita, M. Okano and K. Okamoto, Permeability and Permselectivity of Gases in Fluorinated and Non-fluorinated Polyimides, *Polymer* **33**, 585 (1992).
24. J.O. Hirschfelder, C.F. Curtis and R.B. Bird, *Molecular Theory of Gases and Liquids*, John Wiley, New York (1954).
25. R.C. Reid, J.M. Prausnitz and B.E. Poling, *The Properties of Gases and Liquids*, 4th Edn, McGraw Hill, New York (1987).
26. J.T. Edward, Molecular Volumes and the Stokes–Einstein Equation, *J. Chem. Ed.* **47**, 261 (1970).
27. Y. Nishijima and G. Oster, Diffusion in Concentrated Polymer Solutions, *J. Polym. Sci.* **19**, 337 (1956).
28. R.W. Baker and H.K. Lonsdale, Controlled Release: Mechanisms and Rates, in *Controlled Release of Biological Active Agents*, A.C. Tanquary and R.E. Lacey (eds), Plenum Press, New York, pp. 15–72 (1974).
29. M. Artsis, A.E. Chalykh, N.A. Khalturinskii, W. Moiseev and G.E. Zaikov, Diffusion of Organic Diluents into Ethyl Cellulose, *Eur. Polym. J.* **8**, 613 (1972).
30. A. Bondi, *Physical Properties of Molecular Crystals, Liquids, and Glasses*, Wiley, New York (1968).
31. D.W. Van Krevelen, *Properties of Polymers*, Elsevier, Amsterdam (1990).
32. Y. Kirayama, T. Yoshinaga, Y. Kusuki, K. Ninomiya, T. Sakakibara and T. Tameri, Relation of Gas Permeability with Structure of Aromatic Polyimides, *J. Membr. Sci.* **111**, 169 (1996).
33. C.L. Aitken, W.J. Koros and D.R. Paul, Effect of Structural Symmetry on Gas Transport Properties of Polysulfones, *Macromolecules* **25**, 3424 (1992).
34. J.H. Petropoulos, Mechanisms and Theories for Sorption and Diffusion of Gases in Polymers, in *Polymeric Gas Separation Membranes*, D.R. Paul and Y.P. Yampol'skii (eds), CRC Press, Boca Raton, FL, pp. 17–82 (1994).
35. M.R. Paxton and D.R. Paul, Relationship Between Structure and Transport Properties for Polymers with Aromatic Backbones, in *Polymeric Gas Separation Membranes*, D.R. Paul and Y.P. Yampol'skii (eds), CRC Press, Boca Raton, FL, pp. 83–154 (1994).
36. J.Y. Park and D.R. Paul, Correlation and Prediction of Gas Permeability in Glassy Polymer Membrane Materials via a Modified Free Volume Based Group Contribution Method, *J. Membr. Sci.* **125**, 29 (1997).
37. N.A. Platé and Y.P. Yampol'skii, Relationship between Structure and Transport Properties for High Free Volume Polymeric Materials, in *Polymeric Gas Separation Membranes*, D.R. Paul and Y.P. Yampol'skii (eds), CRC Press, Boca Raton, FL, pp. 155–208 (1994).
38. T. Masuda, Y. Iguchi, B.-Z. Tang and T. Higashimura, Diffusion and Solution of Gases in Substituted Polyacetylene Membranes, *Polymer* **29**, 2041 (1988).
39. S.A. Stern, V.M. Shah and B.J. Hardy, Structure–Permeability Relationships in Silicone Polymers, *J. Polym. Sci., Polym. Phys. Ed.* **25**, 1263 (1987).

40. K. Denbigh, *The Principles of Chemical Equilibrium*, Cambridge University Press, Cambridge (1961).
41. P.G.T. Fogg and W. Gerrard, *Solubility of Gases in Liquids*, Wiley, Chichester (1991).
42. P.J. Flory, *Principles of Polymer Chemistry*, Cornell University Press, Ithaca, NY, p. 511 (1953).
43. B.D. Freeman and I. Pinnau, Polymer Membranes for Gas Separation, *ACS Symp. Ser.* **733**, 6 (1999).
44. R.M. Barrer, J.A. Barrie and J. Slater, Sorption and Diffusion in Ethyl Cellulose, *J. Polym. Sci.* **27**, 177 (1958).
45. A.S. Michaels, W.R. Vieth and J.A. Barrie, Solution of Gases in Polyethylene Terephthalate, *J. Appl. Phys.* **34**, 1 (1963).
46. K. Toi, G. Morel and D.R. Paul, Gas Sorption in Poly(phenylene oxide) and Comparisons with Other Glassy Polymers, *J. Appl. Sci.* **27**, 2997 (1982).
47. W.J. Koros, A.H. Chan and D.R. Paul, Sorption and Transport of Various Gases in Polycarbonate, *J. Membr. Sci.* **2**, 165 (1977).
48. A. Morisato, B.D. Freeman, I. Pinnau and C.G. Casillas, Pure Hydrocarbon Sorption Properties of Poly(1-trimethylsilyl-1-propyne) [PTMSP] and Poly(1-phenyl-1-propyne) [PPP] and PTMSP/PPP Blends, *J. Polym. Sci., Polym. Phys. Ed.* **34**, 1925 (1996).
49. P.M. Bungay, Transport Principles–Porous Membranes, in *Synthetic Membranes: Science Engineering and Applications*, P.M. Bungay, H.K. Lonsdale and M.N. dePintio (eds), D. Reidel, Dordrecht, pp. 109–154 (1986).
50. J.D. Ferry, Ultrafilter Membranes and Ultrafiltration, *Chem. Rev.* **18**, 373 (1936).
51. E.M. Renkin, Filtration, Diffusion and Molecular Sieving Through Porous Cellulose Membranes, *J. Gen. Physiol.* **38**, 225 (1955).
52. R.W. Baker and H. Strathmann, Ultrafiltration of Macromolecular Solutions with High-flux Membranes, *J. Appl. Polym. Sci.* **14**, 1197 (1970).
53. R.C. Lukaszewicz, G.B. Tanny and T.H. Meltzer, Membrane-filter Characterizations and their Implications for Particle Retention, *Pharm. Tech.* **2**, 77 (1978).
54. T.H. Meltzer, *Filtration in the Pharmaceutical Industry*, Marcel Dekker, New York (1987).
55. R.H. Davis and D.C. Grant, Theory for Dead End Microfiltration, in *Membrane Handbook*, W.S.W. Ho and K.K. Sirkar (eds), Van Nostrand Reinhold, New York, pp. 461–479 (1992).
56. D.C. Grant, B.Y.H. Liu, W.G. Fischer and R.A. Bowling, Particle Capture Mechanisms in Gases and Liquids: an Analysis of Operative Mechanisms, *J. Environ. Sci.* **42**, 43 (1989).
57. R.M. Barrer, Diffusion in Porous Media, *Appl. Mater. Res.* **2**, 129 (1963).
58. A.B. Shelekhin, A.G. Dixon and Y.H. Ma, Adsorption, Permeation, and Diffusion of Gases in Microporous Membranes, *J. Membr. Sci.* **75**, 233 (1992).
59. R. Ash, R.M. Barrer and P. Sharma, Sorption and Flow of Carbon Dioxide and Some Hydrocarbons in a Microporous Carbon Membrane, *J. Membr. Sci.* **1**, 17 (1976).
60. S.T. Hwang and K. Kammermeyer, *Techniques of Chemistry, Vol. VII, Membranes in Separations*, Wiley, New York (1975).
61. K. Keizer, A.J. Burggraaf, Z.A.E.P. Vroon and H. Verweij, Two Component Permeation Through Thin Zeolite MFI Membranes, *J. Membr. Sci.* **147**, 159 (1998).
62. M.H. Hassan, J.D. Way, P.M. Thoen and A.C. Dillon, Single Component and Mixed Gas Transport in a Silica Fiber Membrane, *J. Membr. Sci.* **104**, 27 (1995).
63. R. Ash, R.M. Barrer and C.G. Pope, Flow of Adsorbable Gases and Vapours in Microporous Medium, *Proc. R. Soc. London, Ser. A* **271**, 19 (1963).
64. A. Soffer, J.E. Koresh and S. Saggy, Separation Device, US Patent 4,685,940, August 1987.

65. M.B. Rao and S. Sirkar, Nanoporous Carbon Membranes for Separation of Gas Mixtures by Selective Surface Flow, *J. Membr. Sci.* **85**, 253 (1994).
66. M.B. Rao and S. Sirkar, Performance and Pore Characterization of Nanoporous Carbon Membranes for Gas Separation, *J. Membr. Sci.* **110**, 109 (1996).
67. D.Q. Vu, W.J. Koros and S.J. Miller, High Pressure CO_2/CH_4 Separations Using Carbon Molecular Sieve Hollow Fiber Membranes, *Ind. Eng. Chem. Res.* **41**, 367 (2002).
68. N. Tanihara, H. Shimazaki, Y. Hirayama, N. Nakanishi, T. Yoshinaga and Y. Kusuki, Gas Permeation Properties of Asymmetric Carbon Hollow Fiber Membranes Prepared from Asymmetric Polymer Hollow Fibers, *J. Membr. Sci.* **160**, 179 (1999).
69. A.B. Fuertes, Adsorption-selective Carbon Membranes for Gas Separation, *J. Membr. Sci.* **177**, 9 (2000).
70. H. Kita, H. Maeda, K. Tanaka and K. Okamoto, Carbon Molecular Sieve Membranes Prepared from Phenolic Resin, *Chem. Lett.* **179** (1997).
71. I. Pinnau and L.G. Toy, Transport of Organic Vapors through Poly[1-(trimethylsilyl)-1-propyne], *J. Membr. Sci.* **116**, 199 (1996).
72. R. Srinivasan, S.R. Auvil and P.M. Burban, Elucidating the Mechanism(s) of Gas Transport in Poly[1-(trimethylsilyl)-1-propyne] (PTMSP) Membranes, *J. Membr. Sci.* **86**, 67 (1994).
73. J. Cadotte, R. Forester, M. Kim, R. Petersen and T. Stocker, Nanofiltration Membranes Broaden the Use of Membrane Separation Technology, *Desalination* **70**, 77 (1988).
74. S. Egli, A. Ruf and F. Widmer, Entwicklung und Charakterisierung von Kompositmembranen für die Nano- und Ultrafiltration, *Swiss Chem.* **11**(9), 53 (1989).